J. Biochem 2023;173(5):393–411 https://doi.org/10.1093/jb/mvad005

JB THE JOURNAL OF BIOCHEMISTRY

PPARα activation partially drives NAFLD development in liver-specific *Hnf4a*-null mice

Received 19 September 2022; accepted 13 January 2023; published online 23 January 2023

Carlos Ichiro Kasano-Camones[1], Masayuki Takizawa[1], Noriyasu Ohshima[2], Chinatsu Saito[1], Wakana Iwasaki[1], Yuko Nakagawa[3], Yoshio Fujitani[3], Ryo Yoshida[1], Yoshifumi Saito[1], Takashi Izumi[2,4], Shin-Ichi Terawaki[1], Masakiyo Sakaguchi[5], Frank J. Gonzalez[6] and Yusuke Inoue[1,7,†]

[1]Laboratory of Metabolism, Division of Molecular Science, Graduate School of Science and Technology, Gunma University, Kiryu, Gunma 376-8515, Japan ; [2]Department of Biochemistry, Graduate School of Medicine, Gunma University, Maebashi 371-8511, Japan ; [3]Laboratory of Developmental Biology and Metabolism, Institute for Molecular and Cellular Regulation, Gunma University, Maebashi, Gunma 371-8512, Japan ; [4]Faculty of Health Care, Teikyo Heisei University, Tokyo 170-8445, Japan ; [5]Department of Cell Biology, Okayama University Graduate School of Medicine, Dentistry and Pharmaceutical Sciences, Okayama 700-8558, Japan ; [6]Laboratory of Metabolism, Center for Cancer Research, National Cancer Institute, National Institutes of Health, Bethesda, MD 20852, USA; and [7]Gunma University Center for Food Science and Wellness, Maebashi, Gunma 371-8510, Japan

[†]Yusuke Inoue, Laboratory of Metabolism, Division of Molecular Science, Graduate School of Science and Technology, Gunma University, 1-5-1 Tenjin-cho, Kiryu, Gunma 376-8515, Japan. Tel.: +81-277-30-1431, Fax: +81-277-30-1431, email: yinoue@gunma-u.ac.jp

HNF4α regulates various genes to maintain liver function. There have been reports linking HNF4α expression to the development of non-alcoholic fatty liver disease (NAFLD) and non-alcoholic steatohepatitis. In this study, liver-specific *Hnf4a*-deficient mice (*Hnf4a*$^{\Delta Hep}$ mice) developed hepatosteatosis and liver fibrosis, and they were found to have difficulty utilizing glucose. In *Hnf4a*$^{\Delta Hep}$ mice, the expression of fatty acid oxidation-related genes, which are PPARα target genes, was increased in contrast to the decreased expression of PPARα, suggesting that *Hnf4a*$^{\Delta Hep}$ mice take up more lipids in the liver instead of glucose. Furthermore, *Hnf4a*$^{\Delta Hep}$/*Ppara*$^{-/-}$ mice, which are simultaneously deficient in HNF4α and PPARα, showed improved hepatosteatosis and fibrosis. Increased C18:1 and C18:1/C18:0 ratio was observed in the livers of *Hnf4a*$^{\Delta Hep}$ mice, and the transactivation of PPARα target gene was induced by C18:1. When the C18:1/C18:0 ratio was close to that of *Hnf4a*$^{\Delta Hep}$ mouse liver, a significant increase in transactivation was observed. In addition, the expression of *Pgc1a*, a coactivator of PPARs, was increased, suggesting that elevated C18:1 and *Pgc1a* expression could contribute to PPARα activation in *Hnf4a*$^{\Delta Hep}$ mice. These insights may contribute to the development of new diagnostic and therapeutic approaches for NAFLD by focusing on the HNF4α and PPARα signaling cascade.

Graphical Abstract

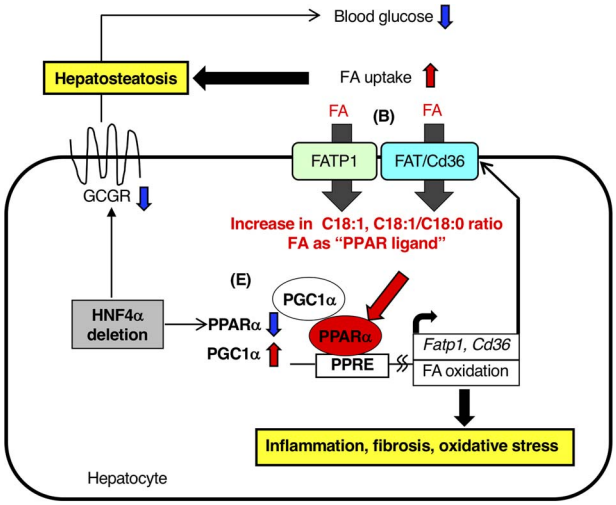

Schematic diagram of NAFLD development in *Hnf4a*$^{\Delta Hep}$ mice

Keywords: Fatty acid, Lipid, Liver, Nuclear receptor, Steatohepatitis.

Abbreviations: HNF4α, hepatocyte nuclear factor 4α; PPARα, peroxisome proliferator-activated receptor α; PGC-1α, peroxisome proliferator-activated receptor γ coactivator 1α; FA, fatty acid; NAFLD, non-alcoholic fatty liver disease; NAFL, non-alcoholic fatty liver; NASH, non-alcoholic steatohepatitis; HCC, hepatocellular carcinoma; Mttp, microsomal triglyceride transfer protein; *Hnf4a*$^{\Delta Hep}$, liver-specific *Hnf4a*-null; *Hnf4a*$^{f/f}$, *Hnf4a*-floxed; *Ppara*$^{-/-}$/*Hnf4a*$^{f/f}$, *Ppara*$^{-/-}$/*Hnf4a*-floxed; *Ppara*$^{-/-}$/*Hnf4a*$^{\Delta Hep}$, *Ppara*$^{-/-}$/liver-specific *Hnf4a*-null; *Pklr*, pyruvate kinase1; Pc, pyruvate carboxylase; Gsy2, glycogen synthase 2; Pygl, glycogen phosphorylase; Pepck1,phosphoenolpyruvate carboxykinase; G6pc1, glucose 6-phosphatase catalytic subunit; ROS, reactive oxidative species; *Gcgr*, glucagon receptor; *Mcad*, medium chain acyl-CoA dehydrogenase; *Cpt2*, paltimoyltransferase; *Acox1*, peroxisomal acyl-CoA dehydrogenase; *Ehhadh*, peroxisomal enoyl-CoA hydratase/3-hydroxyacyl-CoA dehydrogenase; *Acaa1*, peroxisomal 3-oxoacyl-CoA thiolase; *Scad*, mitochondrial short chain acyl-CoA dehydrogenase; *Lcad*, long chain acyl-CoA dehydrogenase; *Vlcad*, very long chain acyl-CoA dehydrogenase; *Ccl2*, C-C motif chemokine ligand 2; *Il1b*, interleukin1β; *Tnfa*, tumor necrosis factor α; ALT, alanine aminotransferase; *Ncf2*, neutrophil cytosolic factor 2; *Sod1*, Cu-Zn superoxidase dismutase; *Gpx1*, glutathione peroxidase 1; *Col1a1*, α-1 type I collagen; *Timp1*, tissue inhibitor of metalloproteinases 1; *Acta2*, α2 *smooth muscle actin; Lpl*, lipoprotein lipase;

Fatp1, fatty acid transporter 1; *Fat/Cd36*, fatty acid translocase; *Acot1*, acyl-CoA thioesterase.

Hepatocyte nuclear factor 4α (HNF4α) is an orphan member of the nuclear receptor superfamily and that is highly expressed in the liver, colon, and intestine *(1)*. HNF4α is an essential factor for hepatocyte differentiation and binds to about 12% of the genes that expressed in human hepatocytes *(2, 3)*. HNF4α was also found to be a master regulator in the liver as revealed by liver-specific *Hnf4a*-null mice (*Hnf4a*$^{\Delta Hep}$ mice) that exhibit many phenotypes due to suppression of many HNF4α target genes *(4–7)*. *Hnf4a*$^{\Delta Hep}$ mice also exhibit hepatosteatosis, probably due to a defect of VLDL secretion through decreased expression of the genes encoding microsomal triglyceride transfer protein (MTTP) and apolipoproteins including APOB, suggesting that HNF4α plays a critical role in lipid homeostasis in liver. In addition, activation of HNF4α in rats fed a high-fat diet improved non-alcoholic fatty liver disease (NAFLD) *(8)*, indicating that HNF4α activation might be a novel drug target for NAFLD.

NAFLD is defined as more than 5% hepatic steatosis and is histologically categorized in benign non-alcoholic fatty liver (NAFL) or progressive non-alcoholic steatohepatitis (NASH) *(9)*. Global prevalence of NAFLD is about 25%, and some NAFLD patients progress to NASH with hepatocyte damage and fibrosis, leading to NASH-related cirrhosis and hepatocellular carcinoma (HCC) *(10, 11)*. Two hits theory was proposed in which the first hit is hepatosteatosis followed by a second hit by some other factors such as reactive oxidative species (ROS), resulting in the development of NASH that is characterized by steatohepatitis and fibrosis *(12)*. Subsequently, a multiple parallel hits hypothesis was proposed in which liver inflammation induced by cytokines from gut and adipose tissues may occur at the same time or even preceding hepatosteatosis *(13)*. The multiple parallel hit hypothesis is effective to understand the pathogenesis of NAFLD/NASH with high diversity, and many studies of NAFLD/NASH have focused on this model. In addition, lipid accumulation is a hallmark of NAFLD, and numerous changes in lipid and fatty acid composition have been implicated in the development of NAFLD/NASH *(14, 15)*.

HNF4α was reported to be associated with NASH *(16)*, and decreased expression of HNF4α was observed in NASH patients and NAFLD model mice such as *ob/ob* mice and mice on a high-fat diet *(17)*. In this model, decreased expression of HNF4α via miR-34a promoted lipid accumulation by suppressing VLDL secretion.

Peroxisome proliferator-activated receptors (PPARs) are nuclear receptors that form heterodimers with retinoid X receptor (RXR) upon binding to their ligands, coincident with binding to peroxisome proliferator response elements (PPREs) on the promoter regions of target genes. The PPAR family consists of three members, PPARα, PPARβ/δ, and PPARγ, that differ in tissue distribution and ligand specificity *(18)*. Of these, PPARα is highly expressed in the liver, heart, and kidney, and is involved in the regulation of lipid transport and catabolism. Fatty acids (FAs) were reported to be endogenous ligands that activate PPARs *(19, 20)*, and many associations between PPARα and NASH have also been described. Various mouse models have been used for non-clinical NASH studies. One of these is a model in which mice are fed a methionine-choline-deficient (MCD) diet, which exhibit phenotypes similar to those of human NASH, including steatohepatitis. *Ppara*$^{-/-}$ mice fed the MCD diet resulted in a more severe phenotype, while wild-type mice fed MCD diet administrated a PPARα agonist had decreased steatohepatitis and liver fibrosis *(21, 22)*. The other model is the *Apoe2* knock-in (*Apoe2*-KI) mice that develop NASH with hepatosteatosis and inflammation when fed a Western high-fat diet *(23)*. These mice are protected from NASH by treatment with a PPARα agonist which reduces hepatosteatosis and accumulation of hepatic macrophage via PPARα activation. Furthermore, *Apoe2*-KI/*Ppara*$^{-/-}$ mice showed a worsened phenotype compared to *Apoe2*-KI mice *(24)*. PPARα agonists suppressed the production of oxidative stress and liver fibrosis in a cirrhosis model rat *(25)*. Thus, in non-clinical studies using mouse models, the usefulness of PPARα agonists for ameliorating NASH-like pathologies was reported in numerous studies.

In this study, liver-specific *Hnf4a*-deficient mice (*Hnf4a*$^{\Delta Hep}$ mice) were found to be NAFLD model mice that develop hepatosteatosis and liver fibrosis. Conversely, *Hnf4a*$^{\Delta Hep}$/*Ppara*$^{-/-}$ mice, which are simultaneously deficient in *Ppara*, showed improvement in these symptoms. In contrast to the decreased expression of *Ppara*, the increased expression of PPARα target genes in *Hnf4a*$^{\Delta Hep}$ mice and the increased binding ability of PPARα to the *Fatp1* promoter, suggesting that PPARα is activated in the liver of *Hnf4a*$^{\Delta Hep}$ mice. Promoter analysis revealed that C18:1 promotes the transcactivation of PPARα together with the increased expression of *Pgc1a* in *Hnf4a*$^{\Delta Hep}$ mice. This finding suggests that the elevated C18:1 might be a critical factor in PPARα activation. Based on these results, a novel model of NAFLD pathogenesis is proposed.

Experimental procedures

Animals

Liver-specific *Hnf4a*-null (*Hnf4a*$^{\Delta Hep}$) and *Hnf4a*-floxed (*Hnf4a*$^{f/f}$) mice were described previously *(4)*. *Ppara*$^{-/-}$/*Hnf4a*-floxed (*Ppara*$^{-/-}$/*Hnf4a*$^{f/f}$) and *Ppara*$^{-/-}$/liver-specific *Hnf4a*-null (*Ppara*$^{-/-}$/*Hnf4a*$^{\Delta Hep}$) mice were generated using *Ppara*-deficient mice *(26)*. All experiments were performed with 45-day-old male *Hnf4a*$^{f/f}$, *Hnf4a*$^{\Delta Hep}$, *Ppara*$^{-/-}$/*Hnf4a*$^{f/f}$, and *Ppara*$^{-/-}$/*Hnf4a*$^{\Delta Hep}$ mice. *Ppara*$^{-/-}$ and the control mice were fed a diet containing 0.1% (wt/wt) Wy-14,643 (Chemsyn Science Laboratories, Lenexa, KS) for 3 days. All mice were housed in a pathogen-free animal facility under standard 12 h light/12 h dark cycle with ad libitum water and chow. All experiments with mice were carried out under the NCI Animal Care and Use Committee and Gunma University Animal Care and Experimentation Committee (Permission number 15-021).

Cell culture

HEK293T, HepG2 and Huh7 cells were cultured at 37 °C in Dulbecco's modified Eagle's medium (Wako, Osaka, Japan) containing 10% fetal bovine serum (HyClone, Logan, UT) and 100 units/ml penicillin and 100 μg/ml streptomycin (Wako).

RNA extraction, reverse-transcription, and quantitative PCR

Total RNA extracted from cell lines and mouse livers using Isogen II (Wako) was transcribed to cDNA using ReverTraAce qPCR RT Master Mix with gDNA Remover (TOYOBO, Osaka, Japan). cDNA was used for quantitative PCR using Luna qPCR Master Mix (New England Biolabs, Tokyo, Japan) with the specific primers on a LightCycler 480 system II (Roche). Levels of mRNA expression were normalized relative to *Gapdh* and *TBP* mRNA as an internal control using ΔΔCt method. Nucleotide sequences of the primers are shown in Supplemental Table 1.

Transfection of siRNA

Ten nM of siRNA against human *HNF4A* mRNA and negative control (Integrated DNA Technologies, Tokyo, Japan) were transfected into HepG2 and Huh7 cells with Lipofectamine RNAiMAX (Life Technologies). After 48 h of transfection, total RNA was harvested. Nucleotide sequences for the siRNA duplexes against human *HNF4A* are follows; rArUrGrGrCrCrArArGrArUrUrGrArCrArArCrCrUrGrUrUGC and rGrCrArArCrArGrGrUrUrGrUrCrArArUrCrUrUrGrGrCrCrArUrGrC.

Cloning of the mouse Fatp1 and Elovl7 promoter regions

The −542 and −444/+52 fragments of the mouse *Fatp1* promoter and +1041, +1207, and +1448/+2240 and +1448/+2106 fragments of the mouse *Elovl7* promoter were amplified with mouse genomic DNA by PCR and cloned into the luciferase reporter vector, pGL4.11 and pGL4.11-HSV-TK mini, respectively *(5, 27)* (Promega, Madison, WI). Mutations were introduced into the PPAR response element located at +2168/+2182 in the *Elovl7* reporter vector by PCR based site-directed mutagenesis. Sequences for the primers are shown in Supplemental Table 2 in the supplemental material.

Transient transfection and luciferase assays

The *Fatp1* and *Elovl7*-cloned pGL4.11 and pGL4.74 encoding *Renilla* luciferase regulated under control of the HSV-TK promoter (Promega) were transfected into HEK293T cells with polyethyleneimine Max (Polyscience, Warrington, PA) as a transfection reagent. For co-transfection, PPARα, PPARβ, PPARγ, RXRα, PGC1α expression plasmids were used. After 24 h, 10 μM of Wy-14,643, 100 nM of GW501516, 5 μM of rosiglitazone, 50 μM of stearate, 50 μM of oleate, 25 μM of stearate and 25 μM of oleate, or 12.5 μM of stearate and 37.5 μM of oleate was added to the medium of transfected cells. After 48 h of transfection, the cells were washed with phosphate-buffered saline (PBS) and promoter activities were measured using Dual-Luciferase Reporter Assay System (Promega). The normalized activity is presented as relative activity based on the promoterless vector.

Liver glycogen contents

Liver glycogen content was determined by a previous described procedure *(28)*.

Histological and immunofluorescent analysis

Livers from $Hnf4a^{f/f}$, $Hnf4a^{\Delta Hep}$, $Ppara^{-/-}/Hnf4a^{f/f}$, and $Ppara^{-/-}/Hnf4a^{\Delta Hep}$ mice were fixed in 10% neutral buffered formalin and embedded in paraffin, and sections cut at a thickness of 3 μm were stained with hematoxylin and eosin (H&E) and Masson Trichrome stain. Immunofluorescent analysis of pancreases from $Hnf4a^{f/f}$ and $Hnf4a^{\Delta Hep}$ was performed using guinea pig polyclonal antibody against insulin (Envision FLEX-Insulin; Dako, Hovedstaden, Denmark) and mouse monoclonal antibody against glucagon (Abcam, Tokyo, Japan). Alexa Fluor 488-conjugated goat anti-guinea pig IgG (Thermo Fisher Scientific, Tokyo) for insulin and Alexa Fluor 594-conjugated goat anti-mouse IgG (Thermo Fisher Scientific) for glucagon were used as secondary antibodies. For nuclear staining, 4′,6-Diamidino-2-phenylindole dihydrochloride (DAPI; DOJIDO, Kumamoto, Japan) was used.

Western blotting

Nuclear protein of liver samples from $Hnf4a^{f/f}$ and $Hnf4a^{\Delta Hep}$ mice were extracted using NE-PER Nuclear and Cytoplasmic Extraction Reagent (Thermo Fisher Scientific), and 20 μg of protein with Laemmli sample buffer was incubated at 65 °C for 15 min, fractionated by 10% SDS-polyacrylamide gel electrophoresis, and blotted onto a PVDF membrane (GE healthcare, Tokyo, Japan). The membrane was incubated for 1 hr with mouse monoclonal antibodies against mouse PPARα (Santa Cruz Biotechnology, Dallas, TX). After washing, the membrane was incubated for 1 h with horseradish peroxidase-conjugated anti-mouse IgG (Cell Signaling Technology, Tokyo, Japan), and the reaction product was visualized using SuperSignal West Pico Chemiluminescent Substrate (Pierce, Rockford, IL) on an ImageQuant LAS4000 (GE healthcare). For confirmation of equal loading of protein, Coomassie Brilliant Blue R-250 stain was performed.

Chromatin immunoprecipitation (ChIP)

ChIP was carried out by use of a previous described procedure *(29)*. ChIP on liver samples was performed according to a protocol using 4 μg of anti-PPARα, PPARβ, PPARγ antibodies and normal mouse IgG (Santa Cruz Biotechnology). Purified DNA was amplified by quantitative PCR using ΔΔCt method. Enrichment of the PPAR response element (PPRE) was normalized to the input samples compared with normal IgG antibody. The following primers were used for real-time PCR; *Fatp1* promoter containing PPRE (74 bp), 5′-CGAAGAAAGAGGAAGGGAGTAGA-3′ and 5′-AACATCTCCTGTGCCCTTTG-3′, *Ehhadh* promoter containing PPRE (74 bp), 5′-TCAGGAGGTAAAGTGTCA GTCG-3′ and 5′-GGAGAGAAGGGGTTGAGGAG-3′, *Hgmcs2* promoter containing PPRE (155 bp), 5′-GACTGATTTCAAGTTCAAGGCTA-3′ and 5′-GCTCA CCATCTGTTCCTAACC-3′, and *Hmgcs2* gene without PPRE as negative controls (74 bp), 5′-GATCCCTGGGAC TCACACA-3′ and 5′- GAATGCACATTTATGGAG GTCA-3′.

Serum analysis

Mice were anesthetized with 2.5% avertin, decapitated, and the trunk blood was collected in a serum separator tube (Becton Dickinson, Franklin Lakes, NJ). The serum was separated by centrifugation at 7000 × g for 5 min and stored at −20 °C prior to analysis. Serum glucose

was measured using Glucometer Elite (Bayer, Elkhart, IN). Serum free fatty acids (Roche Diagnostics, Branchburg, NJ) and triglyceride (Thermo Fisher Scientific) were measured calorimetrically. RIA was used to measure serum insulin, glucagon and adiponectin (Linco Research, St. Charles, MO), corticosterone (ICN Biomedicals, Irvine, CA) and adrenalin (Rocky Mountain Diagnostics, Colorado Springs, CO).

Glucose tolerance test, pyruvate tolerance test, and insulin tolerance test

Hnf4a $^{f/f}$ and *Hnf4a*$^{\Delta Hep}$ mice were fasted overnight for 16 h glucose tolerance test (GTT) and pyruvate tolerance test (PTT) and 6 h insulin tolerance test (ITT) followed by intraperitoneal glucose, pyruvate (2 g/kg body weight), and insulin injection (1.5 U/kg HumulinR, Eli Lilly, Indianapolis, IN). Tail blood was taken at 0, 15, 30, 60, and 120 min after injection and glucose levels were directly measured using automatic glucometer (Bayer).

Analysis of fatty acid composition

Total lipid from *Hnf4a*$^{f/f}$ and *Hnf4a*$^{\Delta Hep}$ mouse liver were extracted by Bligh and Dyer method *(30)*. Briefly, 100 mg of frozen liver tissues were mixed with 3 ml of chloroform/methanol (1:2, v/v) solution. Then, 0.7 ml of distilled water was added. After mixing for 10 min, 1 ml of chloroform were mixed for 10 sec and 1 ml of distilled water was mixed for 10 min. After centrifugation at 2000 rpm for 10 min, about 2 ml of chloroform phase was collected and was evaporated using nitrogen gas and the obtained lipid was resolved in 1 ml of chloroform/methanol (2:1, v/v) solution. Fifty μl of lipid samples were mixed with 100 μl of 1 mM heptadecanoic-17,17,17-d3 acid as an internal reference standard, and was evaporated using nitrogen gas. Dried free fatty acids (FAs), FAs included in lipids, and the standard were methylated by a Fatty Acid Methylation Kit (nacalai tesque, Kyoto, Japan). After centrifugation at 2000 rpm for 10 min, organic phase containing FA methyl esters (FAMEs) was collected. The FAMEs samples, hexane as a blank, Supelco 37 Component FAME Mix (Sigma-Aldrich) containing 37 FAMEs as a quality control were injected into a TQ-8030 gas chromatography–tandem mass spectrometry (GC–MS/MS) system (Shimadzu, Kyoto, Japan) equipped with an AOC-20i autosampler (Shimadzu).

Statistical analysis

All values are expressed as the mean ± standard deviation (S.D.). All data were analyzed by the Mann–Whitney U test for significant differences between the mean values of each group.

Results

Decreased glucose metabolic pathways in Hnf4a $^{\Delta Hep}$ *mice*

Hnf4a $^{\Delta Hep}$ mice tended to exhibit lower blood glucose levels without significant difference using a simple glucometer *(4)*. In the fed state, serum glucose levels in *Hnf4a*$^{\Delta Hep}$ mice were significantly decreased compared to the control, *Hnf4a*$^{f/f}$ mice, while there was no significant difference in glucose levels between *Hnf4a*$^{\Delta Hep}$ mice and *Hnf4a*$^{f/f}$ mice in the fasted state (Fig. 1A). Although there was a significant difference in serum glucose levels between fed and fasted *Hnf4a*$^{f/f}$ mice, there was no significant difference in the glucose levels between fed and fasted *Hnf4a*$^{\Delta Hep}$ mice, indicating that *Hnf4a*$^{\Delta Hep}$ mice had reduced serum glucose in the fed state, but no pathological hypoglycemia during fasting. Thus, expression of mRNAs encoding glucose metabolic enzymes was investigated in the livers of *Hnf4a*$^{\Delta Hep}$ mice (Fig. 1B). In the fed state, hepatic expression of many mRNAs such as pyruvate kinase1 (*Pklr*), pyruvate carboxylase (*Pc*), fructose-1,6-bisphosphatase 1 (*Fbp1*), glycogen synthase 2 (*Gys2*) and glycogen phosphorylase (*Pygl*) was significantly decreased in *Hnf4a*$^{\Delta Hep}$ mice, in agreement with other reports *(31–33)*. In the fasted state, the expression of phosphoenolpyruvate carboxykinase (*Pepck*1) and glucose 6-phosphatase catalytic subunit (*G6pc1*) mRNAs encoding gluconeogenesis enzymes was significantly decreased in *Hnf4a*$^{\Delta Hep}$ mice, indicating that *Hnf4a*$^{\Delta Hep}$ mice might have low gluconeogenesis. Since the expression of *Gys2* and *Pygl* mRNAs was decreased in *Hnf4a*$^{\Delta Hep}$ mice regardless of nutritional state, hepatic glycogen content was investigated (Fig. 1C). There was no significant difference in hepatic glycogen in the fed state, but glycogen content in *Hnf4a*$^{\Delta Hep}$ mice was higher than that in *Hnf4a*$^{f/f}$ mice during fasting. These data suggest that *Hnf4a*$^{\Delta Hep}$ mice might not be able to efficiently degrade glycogen during fasting, partly due to the low expression of *Pygl*. Glucose tolerance test showed that blood glucose levels in *Hnf4a*$^{\Delta Hep}$ mice was much lower than those in *Hnf4a*$^{f/f}$ mice (Fig. 1D), indicating that *Hnf4a*$^{\Delta Hep}$ mice are more glucose tolerant than *Hnf4a*$^{f/f}$ mice. Since the expression of genes such as *Pc*, *Pepck1* and *G6pc1* that are involved in gluconeogenesis was decreased in *Hnf4a*$^{\Delta Hep}$ mice during fasting, pyruvate tolerance test was investigated using pyruvate as a substrate of gluconeogenesis (Fig. 1E). As expected, blood glucose levels in *Hnf4a*$^{\Delta Hep}$ mice were lower than those in *Hnf4a*$^{f/f}$ mice. Furthermore, *Hnf4a*$^{\Delta Hep}$ mice were found to be insulin resistant because their blood glucose levels were higher than those in *Hnf4a*$^{f/f}$ mice as revealed by insulin tolerance test (Fig. 1F).

Hnf4a$^{\Delta Hep}$ *mice exhibit decreased expression of the glucagon receptor*

Various factors such as body weight and levels of serum free fatty acid (FFA) and hormones were investigated. There was no significant difference in the levels of body weight, serum FFA, adiponectin, and adrenaline between *Hnf4a*$^{f/f}$ and *Hnf4a*$^{\Delta Hep}$ mice (Fig. 2A-D). Serum corticosterone levels were increased in fed *Hnf4a*$^{\Delta Hep}$ mice, but there was no significant difference in fasted *Hnf4a*$^{\Delta Hep}$ mice (Fig. 2E). Furthermore, serum glucagon levels were higher in *Hnf4a*$^{\Delta Hep}$ mice in spite of the nutrient states (Fig. 2F). Although glucagon receptor (GCGR) is highly expressed in the liver, hepatic expression of *Gcgr* mRNA was very low in *Hnf4a*$^{\Delta Hep}$ mice (Fig. 2G). To investigate whether HNF4α directly transactivates *GCGR* expression in humans, HNF4α was overexpressed or suppressed in Huh7 and HepG2 cells that highly express endogenous HNF4α (Fig. 2H). Overexpression of HNF4α strongly induced *GCGR* mRNA in both cell lines (Fig. 2H, upper panel), but no suppression of *GCGR* was observed in

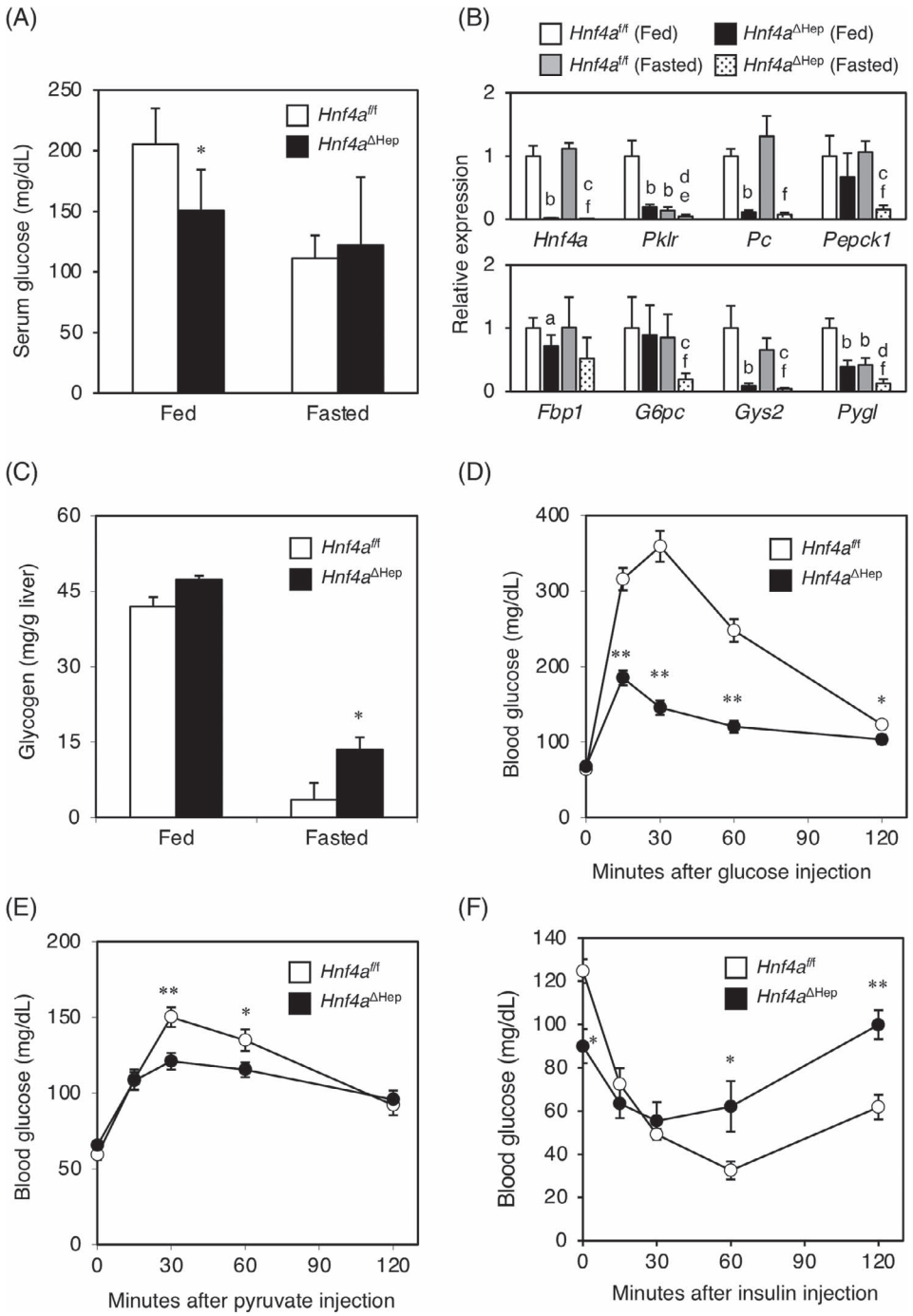

Fig. 1. Analysis of glucose-related phenotype and gene expression in *Hnf4a* $^{\Delta Hep}$ mice. (A) Serum glucose levels in fed and 16 h-fasted *Hnf4a*$^{f/f}$ and *Hnf4a*$^{\Delta Hep}$ mice ($n = 6$ for each genotype). Data are mean ± S.D. *, $P < 0.05$ compared to fed *Hnf4a*$^{f/f}$ mice. (B) Quantitative RT-PCR from total liver RNA of fed and 16 h-fasted *Hnf4a*$^{f/f}$ and *Hnf4a*$^{\Delta Hep}$ mice ($n = 5$ for each genotype). Hepatic gene expression involved in glycolysis, glycogenolysis, glycogenesis, and gluconeogensis was investigated. Data are mean ± S.D. [a], $P < 0.05$; [b], $P < 0.01$ compared to fed *Hnf4a*$^{f/f}$ mice. [c], $P < 0.05$; [d], $P < 0.01$ compared to fed *Hnf4a*$^{\Delta Hep}$ mice. [e], $P < 0.05$; [f], $P < 0.01$ compared to fasted *Hnf4a*$^{f/f}$ mice. (C) Hepatic glycogen levels in fed and 16 h-fasted *Hnf4a*$^{f/f}$ and *Hnf4a*$^{\Delta Hep}$ mice ($n = 6$ for each genotype). Data are mean ± S.D. *, $P < 0.01$ compared to fasted *Hnf4a*$^{f/f}$ mice. (D) Glucose tolerance test at 45-day-old *Hnf4a*$^{f/f}$ and *Hnf4a*$^{\Delta Hep}$ mice ($n = 20$ for each genotype). Data are mean ± S.D. *, $P < 0.01$; **, $P < 0.001$ compared to *Hnf4a*$^{f/f}$ mice. (E) Pyruvate tolerance test at 45-day-old *Hnf4a*$^{f/f}$ and *Hnf4a*$^{\Delta Hep}$ mice ($n = 15$ for each genotype). Data are mean ± S.D. *, $P < 0.01$; **, $P < 0.001$ compared to *Hnf4a*$^{f/f}$ mice. (F) Insulin tolerance test at 45-day-old *Hnf4a*$^{f/f}$ and *Hnf4a*$^{\Delta Hep}$ mice ($n = 8$ for each genotype). Data are mean ± S.D. *, $P < 0.01$; **, $P < 0.001$ compared to *Hnf4a*$^{f/f}$ mice.

these cells by RNA interreference of HNF4α (Fig. 2H, lower panel). These results indicate that *GCGR* expression might be partially regulated by HNF4α, but the regulation of *GCGR* by HNF4α is more complicated. In addition, glucagon preferentially accumulated in islets of *Hnf4a*$^{\Delta Hep}$ mice compared to *Hnf4a*$^{f/f}$ mice (Fig. 2I), indicating that serum glucagon levels would be increased due to lack of *Gcgr* expression in *Hnf4a*$^{\Delta Hep}$ mice.

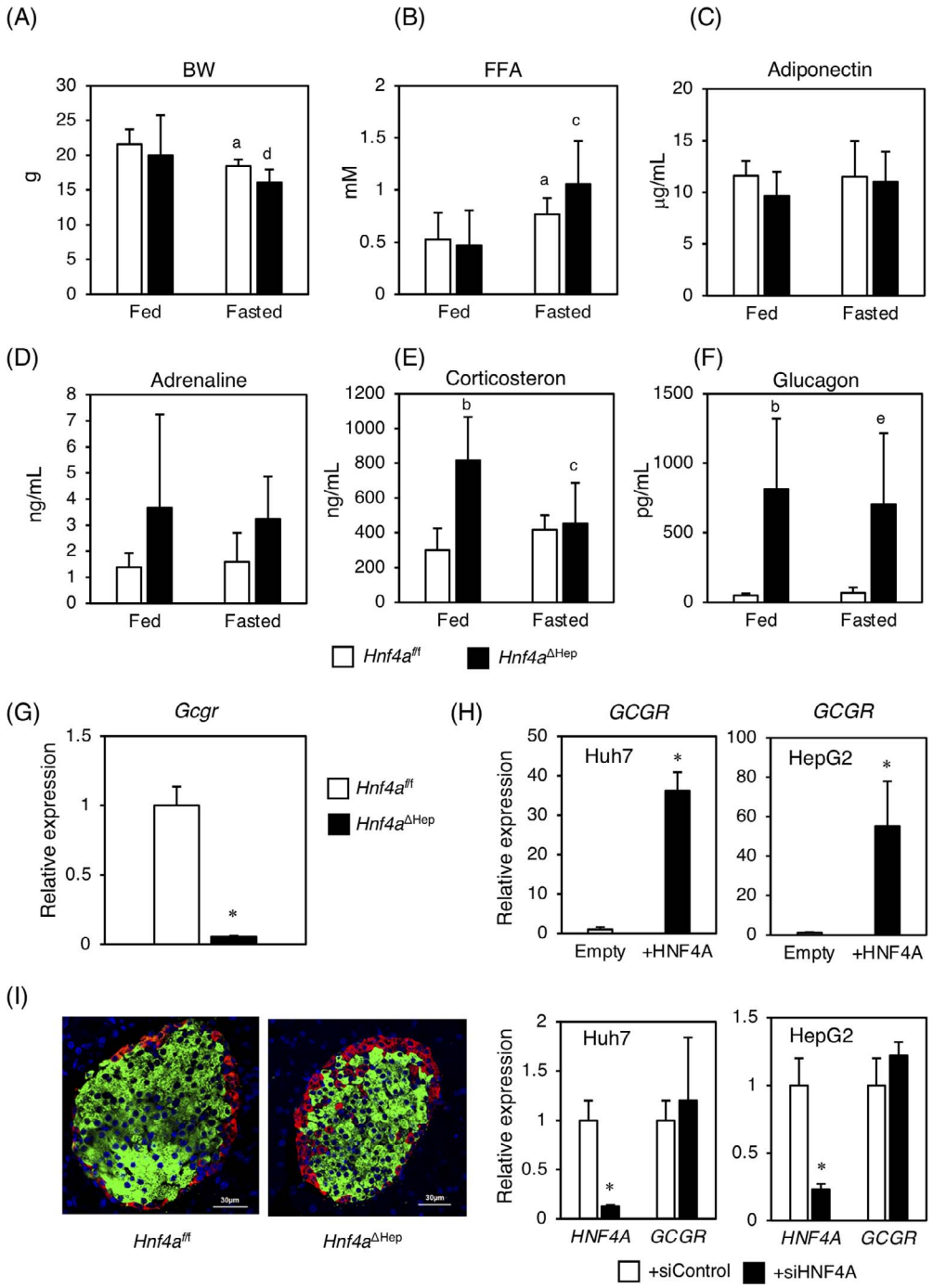

Fig. 2. Serum chemistry profile, expression of *Gcgr*, and immunostaining of glucagon. Body wight (A), serum levels of FFA (B), adiponection (C), adrenaline (D), cortisterone (E), and glucagon (F) in fed and 16 h-fasted *Hnf4a*$^{f/f}$ and *Hnf4a*$^{\Delta Hep}$ mice ($n = 7$ for each genotype). Data are mean ± S.D. [a], $P < 0.05$; [b], $P < 0.01$ compared to fed *Hnf4a*$^{f/f}$ mice. [c], $P < 0.05$ compared to fed *Hnf4a*$^{\Delta Hep}$ mice. [d], $P < 0.05$; [e], $P < 0.01$ compared to fasted *Hnf4a*$^{f/f}$ mice. (G) Quantitative RT-PCR of glucogon receptor (*Gcgr*) from total liver RNA of fed *Hnf4a*$^{f/f}$ and *Hnf4a*$^{\Delta Hep}$ mice. Data are mean ± S.D. *, $P < 0.01$ compared to *Hnf4a*$^{f/f}$ mice. (H) Quantitative RT-PCR from total RNA of HepG2 and Huh7 cells transfected empty, and HNF4α expression vector (*upper*), and negative control of siRNA (siControl), and siRNA for HNF4α (siHNF4A) (*lower*). The normalized expression in the cells transfected HNF4α expression vector and siHNF4A is presented relative to that in the cells transfected empty vector and siControl. Data are mean ± S.D. *, $P < 0.01$ compared to empty vector and siControl-transfected cells. (I) Immunofluorescence staining of pancreatic insulin (green), glucagon (red), and 4′,6-diamidino-2-phenylindole (DAPI) (blue) in fed *Hnf4a*$^{f/f}$ *(left) and Hnf4a*$^{\Delta Hep}$ mice (right).

Disruption of PPARα in Hnf4a$^{\Delta Hep}$ *mice improves hepatosteatosis*

Hnf4a $^{\Delta Hep}$ mice exhibit lower glucose levels, probably due to low gluconeogenesis, indicating that they might use more FA as an energy source rather than glucose. It was reported that hepatic expression of medium chain acyl-CoA dehydrogenase (*Mcad*) and carnitine paltimoyltransferase (*Cpt2*) that are involved in FA β-oxidation is increased in *Hnf4a*$^{\Delta Hep}$ mice *(4)*. In addition, hepatic expression of the genes encoding peroxisomal enoyl-CoA, hydratase/

3-hydroxyacyl-CoA dehydrogenase (*Ehhadh*) and *Cyp4a14* that are involved in FA β- and ω-oxidation in peroxisomes and endoplasmic reticulum, respectively, and 3-hydroxy-3-methylglutaryl-CoA synthase 2 (*Hmgcs2*) involved in ketogenesis was significantly increased in $Hnf4a^{\Delta Hep}$ mice (Fig. 3A). Expression of pyruvate dehydrogenase kinase 4 (*Pdk4*) that plays a key role in glucose and fatty acid metabolism was markedly increased in $Hnf4a^{\Delta Hep}$ mice, suggesting that hepatic energy source would be converted from glucose to fatty acid in $Hnf4a^{\Delta Hep}$ mice. Expression of *Mcad* and long chain acyl-CoA dehydrogenase (*Lcad*) mRNAs encoding enzymes involved in FA β-oxidation in mitochondria, tended to increase in $Hnf4a^{\Delta Hep}$ mice, while expression of peroxisomal acyl-CoA dehydrogenase (*Acox1*), peroxisomal 3-oxoacyl-CoA thiolase (*Acaa1*), mitochondrial short chain acyl-CoA dehydrogenase (*Scad*), and very long chain acyl-CoA dehydrogenase (*Vlcad*) mRNAs remained unchanged between $Hnf4a^{f/f}$ and $Hnf4a^{\Delta Hep}$ mice. Although they are target genes for PPARα, hepatic expression of *Ppara* mRNA was surprisingly decreased in $Hnf4a^{\Delta Hep}$ mice *(4)*. The PPAR family consisted of three isoforms, PPARα, PPARβ/δ and PPARγ. Hepatic expression of *Ppara* mRNA was decreased by about half in $Hnf4a^{\Delta Hep}$ mice, while expression of *Pparb*, and *Pparg* mRNAs remained unchanged between $Hnf4a^{f/f}$ and $Hnf4a^{\Delta Hep}$ mice (Fig. 3B). In addition, the levels of PPARγ coactivator 1α (*Pgc1a*) mRNA encoding a coactivator of all PPARs, was significantly increased in $Hnf4a^{\Delta Hep}$ mice. Furthermore, PPARα protein was markedly reduced in $Hnf4a^{\Delta Hep}$ mice (Fig. 3C). These results indicate that expression of PPARα protein is reduced, but PPARα might be superactivated in $Hnf4a^{\Delta Hep}$ mice to induce expression of the target genes. Thus, mice lacking hepatic expression of both HNF4α and PPARα were generated ($Hnf4a^{\Delta Hep}/Ppara^{-/-}$ mice). Hepatosteatosis in $Hnf4a^{\Delta Hep}$ mice was clearly improved by the loss of PPARα (Fig. 3D). In addition, Masson trichrome staining revealed that liver fibrosis induced in $Hnf4a^{\Delta Hep}$ mice was also impaired in $Hnf4a^{\Delta Hep}/Ppara^{-/-}$ mice (Fig. 3E). Thus, hepatosteatosis and liver fibrosis observed in $Hnf4a^{\Delta Hep}$ mice could be caused by a combination of lack of HNF4α and concurrent activation of PPARα.

Elevated inflammation, oxidative stress and fibrosis markers in $Hnf4a^{\Delta Hep}$ mice

Since $Hnf4a^{\Delta Hep}$ mice exhibit liver fibrosis, hepatic expression of NASH associated markers involved in inflammation, oxidative stress and fibrosis was investigated. The mRNA expression of C-C motif chemokine ligand 2 (*Ccl2*), which regulates migration and accumulation of monocyte and macrophage *(34)*, and interleukin1β (*Il1b*), an inflammatory cytokine playing the central role in the induction of inflammatory reaction, early immune response and cell death *(35)*, was significantly increased in the livers of $Hnf4a^{\Delta Hep}$ mice, and decreased in $Hnf4a^{\Delta Hep}/Ppara^{-/-}$ mice compared to that in $Hnf4a^{\Delta Hep}$ mice (Fig. 4A). Expression of other inflammation markers such as tumor necrosis factor α (*Tnfa*) mRNA was similar between $Hnf4a^{\Delta Hep}$ mice and $Hnf4a^{\Delta Hep}/Ppara^{-/-}$ mice. This suggests that inflammation was promoted in $Hnf4a^{\Delta Hep}$ mice liver, in agreement with an early study revealing that the levels of serum alanine aminotransferase (ALT) were increased about 1.6-fold in $Hnf4a^{\Delta Hep}$ mice *(4)*. Expression of mRNA encoding neutrophil cytosolic factor 2 (*Ncf2*), subunits of NADPH oxidase complex type 2 (Nox2 complex) that produce reactive oxygen species (ROS), was also significantly increased in $Hnf4a^{\Delta Hep}$ mice and was decreased in $Hnf4a^{\Delta Hep}/Ppara^{-/-}$ mice (Fig. 4B). Expression of *Ncf1* mRNA was similar between $Hnf4a^{\Delta Hep}$ mice and $Hnf4a^{\Delta Hep}/Ppara^{-/-}$ mice, indicating that oxidative stress would accumulate in $Hnf4a^{\Delta Hep}$ mice likely because the mRNAs encoding catalase, Cu-Zn superoxidase dismutase (*Sod1*) and glutathione peroxidase 1 (*Gpx1*) that protect cells against oxidative damage were decreased in $Hnf4a^{\Delta Hep}$ mice *(5)*. In addition, the expression of mRNAs of transforming growth factor β1 (*Tgfb1*) involved in the production of extracellular matrix (ECM) such as collagen and fibronectin, α-1 type I collagen (*Col1a1*), tissue inhibitor of metalloproteinases 1 (*Timp1*), and *Timp3* was significantly increased in $Hnf4a^{\Delta Hep}$ mice (Fig. 4C). These mRNAs, except *Tgfb1*, were decreased in $Hnf4a^{\Delta Hep}/Ppara^{-/-}$ mice. Levels of another fibrosis marker gene mRNA, α2 smooth muscle actin (*Acta2*) was similarly increased in $Hnf4a^{\Delta Hep}$ mice and decreased in $Hnf4a^{\Delta Hep}/Ppara^{-/-}$ mice. These results are consistent with the development of liver fibrosis in $Hnf4a^{\Delta Hep}$ mice as shown in Fig. 3E. Thus, the expression of genes involved in inflammation, oxidative stress and fibrosis, the markers of NASH, was increased in $Hnf4a^{\Delta Hep}$ mice and decreased in $Hnf4a^{\Delta Hep}/Ppara^{-/-}$ mice.

In an earlier study, $Hnf4a^{\Delta Hep}$ mice exhibited reduced expression of hepatic apoproteins and microsomal triglyceride transfer protein (MTTP) that are encoded by HNF4α target genes *(36, 37)*, indicating that $Hnf4a^{\Delta Hep}$ probably cannot export lipid from hepatocytes, which may partially contributes to hepatosteatosis. However, some expression of PPARα target genes involved in FA oxidation were increased in $Hnf4a^{\Delta Hep}$ mice (Fig. 3A), indicating that the increased expression of FA oxidation-related genes in $Hnf4a^{\Delta Hep}$ mice might conversely inhibit hepatosteatosis. Thus, expression of other PPARα target genes was further investigated. Hepatic expression of mRNAs encoding lipoprotein lipase (*Lpl*), FA transporter 1 (*Fatp1*), FA translocase (*Fat/Cd36*) and acyl-CoA thioesterase (*Acot1*) that are involved in extracellular degradation of triglyceride, uptake of long-chain FAs and hydrolysis of acyl-CoA, respectively *(27, 38, 39)*, was increased in $Hnf4a^{\Delta Hep}$ mice, and expression of *Fatp1* and *Fat/Cd36* mRNA was increased about 20-fold in $Hnf4a^{\Delta Hep}$ mice (Fig. 4D). In addition, the expression of *Fatp1* and *Fat/Cd36* mRNAs in $Hnf4a^{\Delta Hep}/Ppara^{-/-}$ mice was strongly suppressed compared to those in $Hnf4a^{\Delta Hep}$ mice. These results indicate that increased uptake of long-chain FAs by FATP1 and FAT/CD36 might be another reason for hepatosteatosis in $Hnf4a^{\Delta Hep}$ mice.

$Hnf4a^{\Delta Hep}/Ppara^{-/-}$ mice markedly improved hepatosteatosis, but hepatic expression of *Ppara* mRNA was decreased in $Hnf4a^{\Delta Hep}$ mice (Fig. 3B and C). Thus, transactivation of PPARα target genes might be due to PPARβ/δ and PPARγ. While there was no change of PPARβ/δ and PPARγ expression between $Hnf4a^{f/f}$ and $Hnf4a^{\Delta Hep}$ mice, activation of PPARβ/δ and/or PPARγ could activate their target genes. Since *Fatp1* mRNA was markedly increased in $Hnf4a^{\Delta Hep}$ mice (Fig. 4C), and

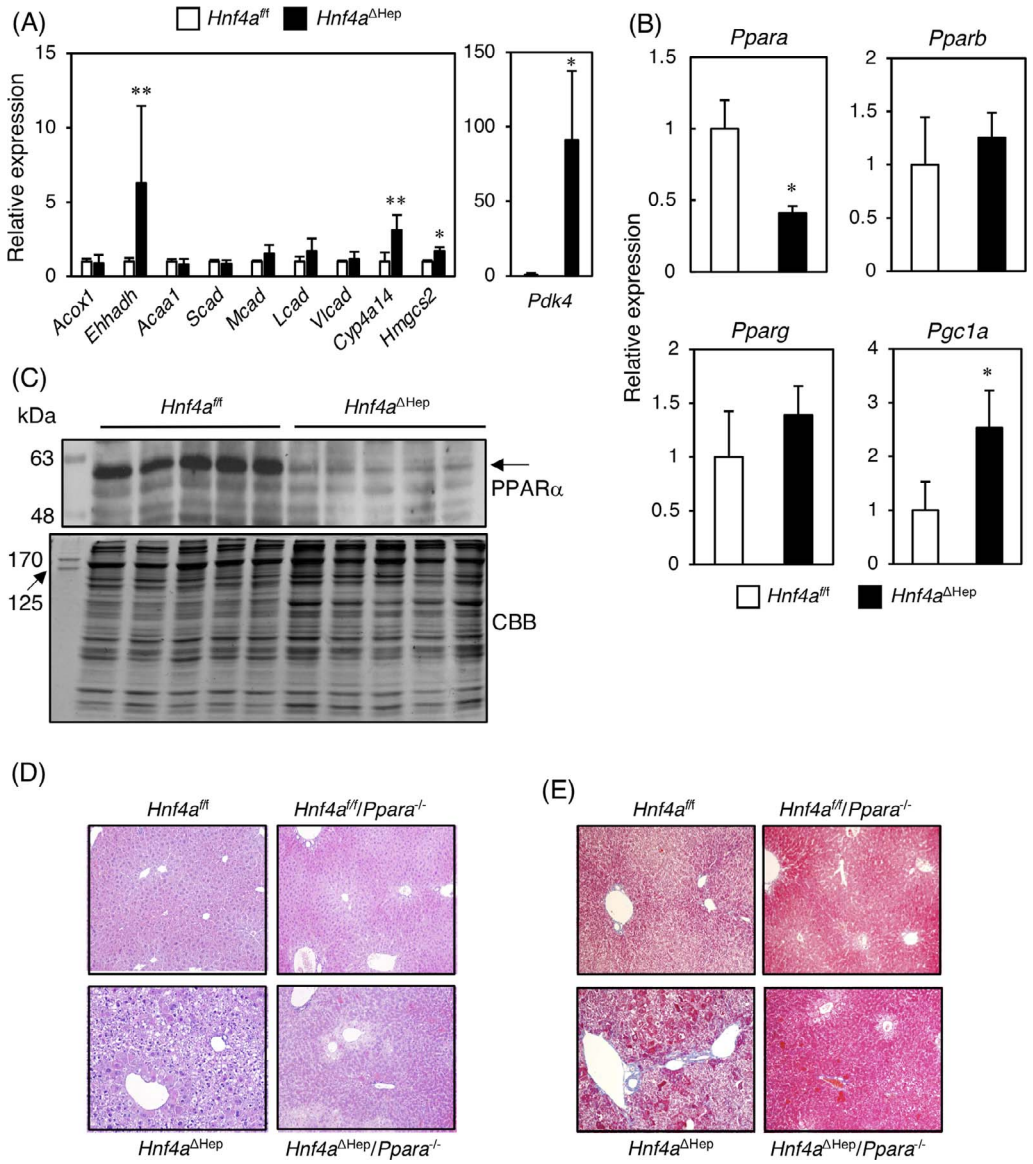

Fig. 3. Expression of PPARs and PPAR target genes, and improvement of hepatosteatosis and fibrosis. (A) Quantitative RT-PCR from total liver RNA of *Hnf4a*$^{f/f}$ and *Hnf4a*$^{\Delta Hep}$ mice ($n = 5$ for each genotype). Data are mean ± S.D. *, $P < 0.05$; **, $P < 0.01$ compared to *Hnf4a*$^{f/f}$ mice. (B) Quantitative RT-PCR from total liver RNA of *Hnf4a*$^{f/f}$ and *Hnf4a*$^{\Delta Hep}$ mice ($n = 5$ for each genotype). Data are mean ± S.D. *, $P < 0.05$ compared to *Hnf4a*$^{f/f}$ mice. (C) Western blot of PPARA protein from nuclear extracts of *Hnf4a*$^{f/f}$ and *Hnf4a*$^{\Delta Hep}$ mice ($n = 5$ for each genotype). Equal loading was confirmed by coomassie brilliant blue (CBB) stain. Representative images of HE staining (D) and Masson Trichrome stain (E) of liver sections of *Hnf4a*$^{f/f}$, *Hnf4a*$^{\Delta Hep}$, *Hnf4a*$^{f/f}$/*Ppara*$^{-/-}$, and *Hnf4a*$^{\Delta Hep}$/*Ppara*$^{-/-}$ mice.

Fatp1 mRNA was reported to be transactivated by all PPARs *(27)*, promoter analysis was performed to determine whether PPARs transactivate the *Fatp1* in the presence of PGC1α whose expression was increased in *Hnf4a*$^{\Delta Hep}$ mice. The *Fatp1* promoter with a PPAR responsive element (PPRE) at −492/−476 was transactivated by all PPARs in the presence of the ligands, Wy-14,643 for PPARα, GW501516 for PPARβ/δ and rosiglitazone for PPARγ compared to the *Fatp1* promoter without the PPAR responsive element (-PPRE) (Fig. 5A-D). In addition, inclusion of PGC1α with all PPARs transactivated the *Fatp1* promoter more strongly in the presence of the ligands, and the transactivation of the *Fatp1* promoter by PPARα was the strongest among three PPARs. Thus, binding of PPARs to PPRE of the *Fatp1* promoter was investigated by chromatin immunoprecipitation (ChIP), revealing that PPARα binds to the PPRE of the *Fatp1* promoter in the livers of *Hnf4a*$^{\Delta Hep}$ mice, while no binding of PPARβ/δ and PPARγ to the *Fatp1* promoter was observed (Fig. 5E). As positive controls, PPARα was found to bind to the PPRE of the *Ehhadh and Hmgcs2* promoters that are PPARα targets in the livers of *Hnf4a*$^{\Delta Hep}$ mice, but not *Hnf4a*$^{f/f}$ mice. These results indicate that hepatic PPARα, but not PPARβ/δ and PPARγ directly and physiologically binds to the *Fatp1* promoter and thus might be transactivated in *Hnf4a*$^{\Delta Hep}$ mice.

Altered FA composition and FA desaturase and elongase expression in Hnf4a$^{\Delta Hep}$ *mice*

Since PPARα is activated by endogenous FAs, changing of FA composition might be essential for activation of PPARα in *Hnf4a*$^{\Delta Hep}$ mice. To explore this question, total

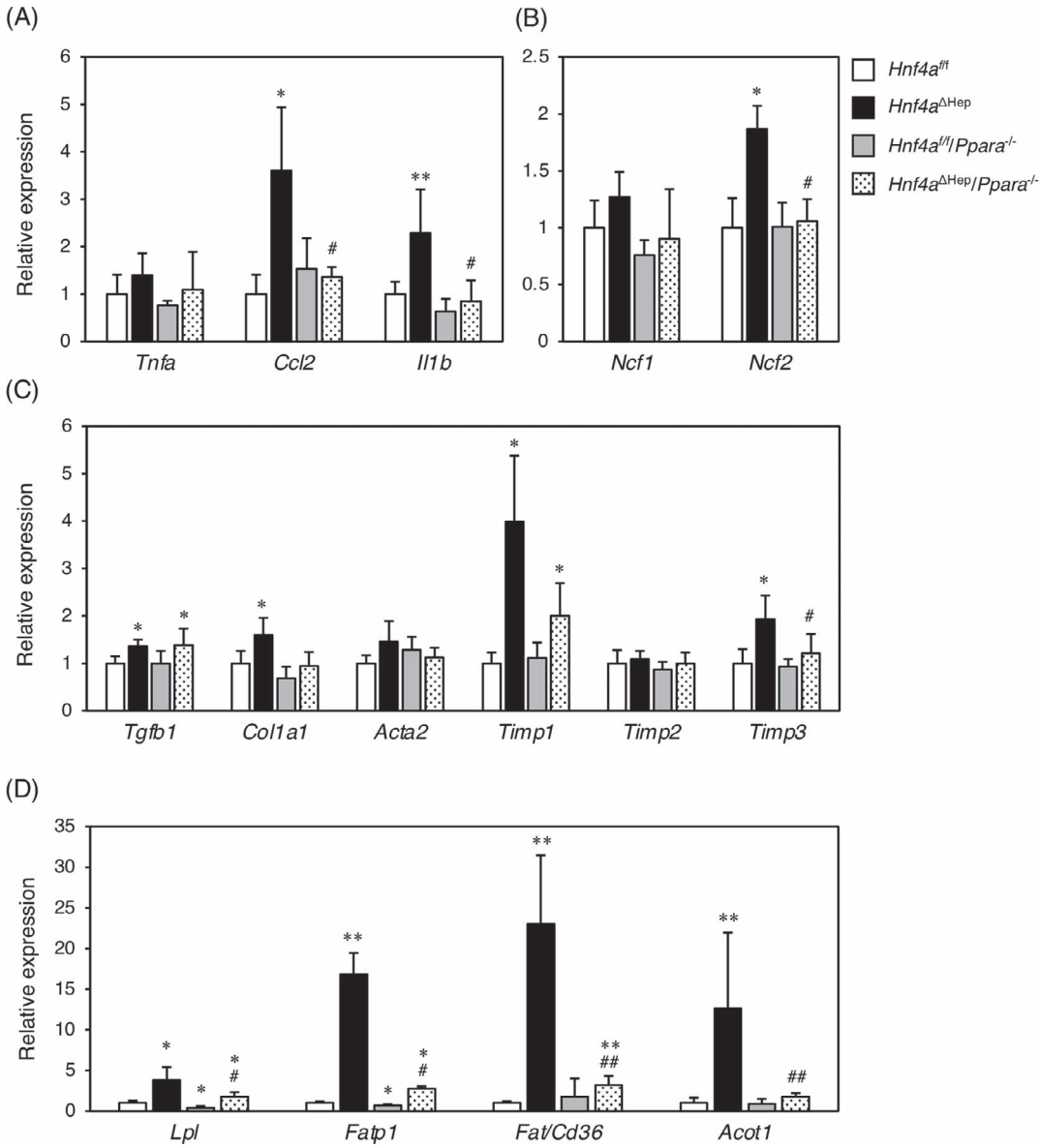

Fig. 4. Expression of inflammation, oxidative stress, and fibrosis marker genes and PPAR target genes involved in FA metabolism in *Hnf4a*$^{f/f}$ *and Hnf4a*$^{\Delta Hep}$, *Hnf4a*$^{f/f}$*/Ppara*$^{-/-}$, and *Hnf4a*$^{\Delta Hep}$*/Ppara*$^{-/-}$ mice. Quantitative RT-PCR of inflammation (A), oxidative stress (B), fibosis markers (C), and PPAR target genes involved in fatty aicd mtatabosim (D) from total liver RNA of *Hnf4a*$^{f/f}$, *Hnf4a*$^{\Delta Hep}$, *Hnf4a*$^{f/f}$*/Ppara*$^{-/-}$, and *Hnf4a*$^{\Delta Hep}$*/Ppara*$^{-/-}$ mice ($n = 5$ for each genotype). Data are mean ± S.D. *, $P < 0.05$; **, $P < 0.01$ compared to *Hnf4a*$^{f/f}$ mice. #, $P < 0.05$; ##, $P < 0.01$ compared to *Hnf4a*$^{\Delta Hep}$ mice.

lipids from the livers of *Hnf4a*$^{f/f}$ and *Hnf4a*$^{\Delta Hep}$ mice were extracted and the FA composition was measured (Fig. 6). Of thirty-nine FA used, 14 FAs with more than 16 carbons were found at measurable levels in liver (Fig. 6A). Oleate (C18:1), linoleate (C18:2), and C20 unsaturated icosenoate (C20:1) and icosadienoate (C20:2) were increased, while margarate (C17:0), stearate (C18:0) and C20 saturated and unsaturated arachisate (C20:0), eicosatrienoate (C20:3), arachidonate (C20:4) and eicosapentaenoate (C20:5) were decreased in *Hnf4a*$^{\Delta Hep}$ mice compared to *Hnf4a*$^{f/f}$ mice (Fig. 6B). Among the major FAs, C18 saturated C18:0 was decreased in *Hnf4a*$^{\Delta Hep}$ mice, and C18 unsaturated C18:1 and C18:2 in *Hnf4a*$^{\Delta Hep}$ mice were increased about 2.2- and 1.5-fold compared to *Hnf4a*$^{f/f}$ mice, respectively.

FA composition is regulated by FA desaturase and elongase. To investigate the reason why FA composition is altered in *Hnf4a*$^{\Delta Hep}$ mice, hepatic mRNA expression encoding FA desaturases and elongases was analyzed. As for FA desaturase, the expression of FA desaturase 2 (*Fads2*) and *Fads6* mRNAs was significantly decreased in *Hnf4a*$^{\Delta Hep}$ and *Hnf4a*$^{\Delta Hep}$*/Ppara*$^{-/-}$ mice compared to that in *Hnf4a*$^{f/f}$ mice (Fig. 7A). Expression of *Fads3* mRNA was markedly increased in *Hnf4a*$^{\Delta Hep}$ mice compared to that in *Hnf4a*$^{f/f}$ mice, but was conversely decreased in *Hnf4a*$^{\Delta Hep}$*/Ppara*$^{-/-}$ compared to that in *Hnf4a*$^{\Delta Hep}$ mice. Thus, only the expression of *Fads3* mRNA showed conflicting results between *Hnf4a*$^{\Delta Hep}$ and *Hnf4a*$^{\Delta Hep}$*/Ppara*$^{-/-}$ mice. As for FA elongase, elongation of very long chain FA

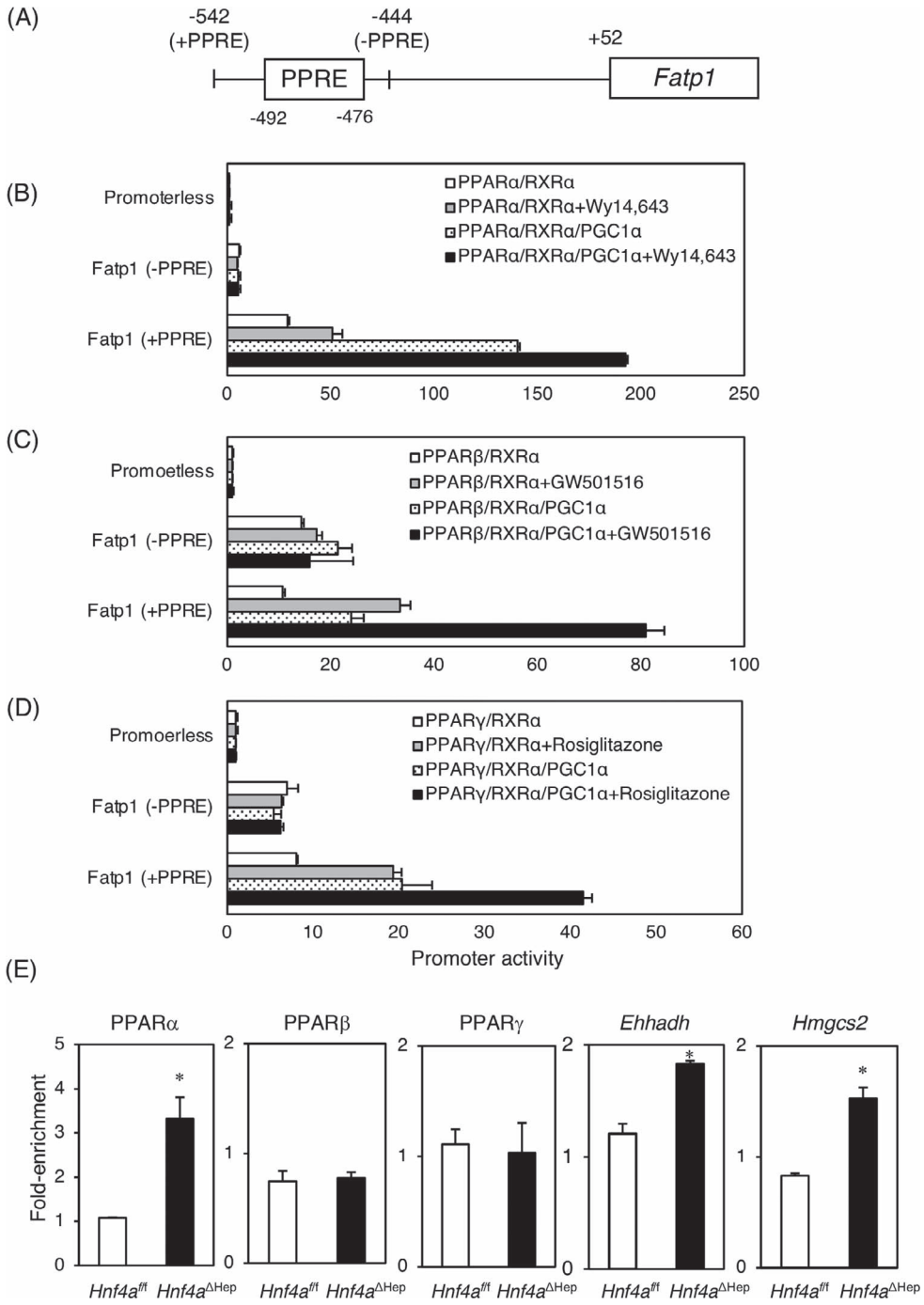

Fig. 5. Promoter analysis of the *Fatp*1 gene by PPARs and the binding of PPARs to PPRE of the *Fatp*1. (A) Schematic diagram of the promoter of the *Fatp1* gene. PPAR response element (PPRE) locates at −542/−444 from the transcrition start site. Promoter constructs of promoterless, the *Fatp1* gene with and without PPRE (−444/+52; (-PPRE) and − 542/+52; (+PPRE)) were transfected into HEK293T cells. At that time, PPARα (B), PPARβ/δ (C), and PPARγ (D) expression vector was co-transfected with PGC1α expression vector in the absence and presence of the ligand of PPARα (10 μM Wy-14,643), PPARβ/δ (100 nM GW501516), and PPARγ (5 μM rosiglitazone), respectively. The normalized activity is presented as relative activity based on the promoterless vector. Error bars represent as S.D. Data are mean ± S.D. of three independent experiments. (E) Chromatin immunoprecipitation using the livers of *Hnf4a*$^{f/f}$ and *Hnf4a*$^{\Delta Hep}$ mice with 4 μg of anti-PPARα, PPARβ/δ, and PPARγ antibodies and normal goat IgG. The regions between −538 and − 465 containing the PPRE in the *Fatp1* promoter, between −2899 and − 2833 containing the PPRE in the *Ehhadh* promoter, between −513 and − 358 containing the PPRE in the *Hmgcs2* promoter, and between +45,820 and + 45,893 without an PPRE in the mouse *Hmgcs2* gene were amplified, respectively. For the *Ehhadh* and *Hmgcs*2 promoters containing the PPRE, only anti-PPARα antibody was used. The data from qPCR was normalized relative to the input and expressed as -fold enrichment over data from IgG control. Error bars represent S.D. Data are mean ± S.D. of three independent experiments. *, $P < 0.05$ compared to *Hnf4a*$^{f/f}$ mice.

1–7 (ELOVL1–7), expression of *Elovl1*, *Elovl2* and *Elovl5* mRNAs was significantly decreased to the same extent, and expression of *Elovl3* mRNA was hardly detected in *Hnf4a*$^{\Delta Hep}$ and *Hnf4a*$^{\Delta Hep}$*/Ppara*$^{-/-}$ mice compared to that in *Hnf4a*$^{f/f}$ (Fig. 7B). Conversely, since expression of *Elovl7* mRNA was largely increased in *Hnf4a*$^{\Delta Hep}$ and

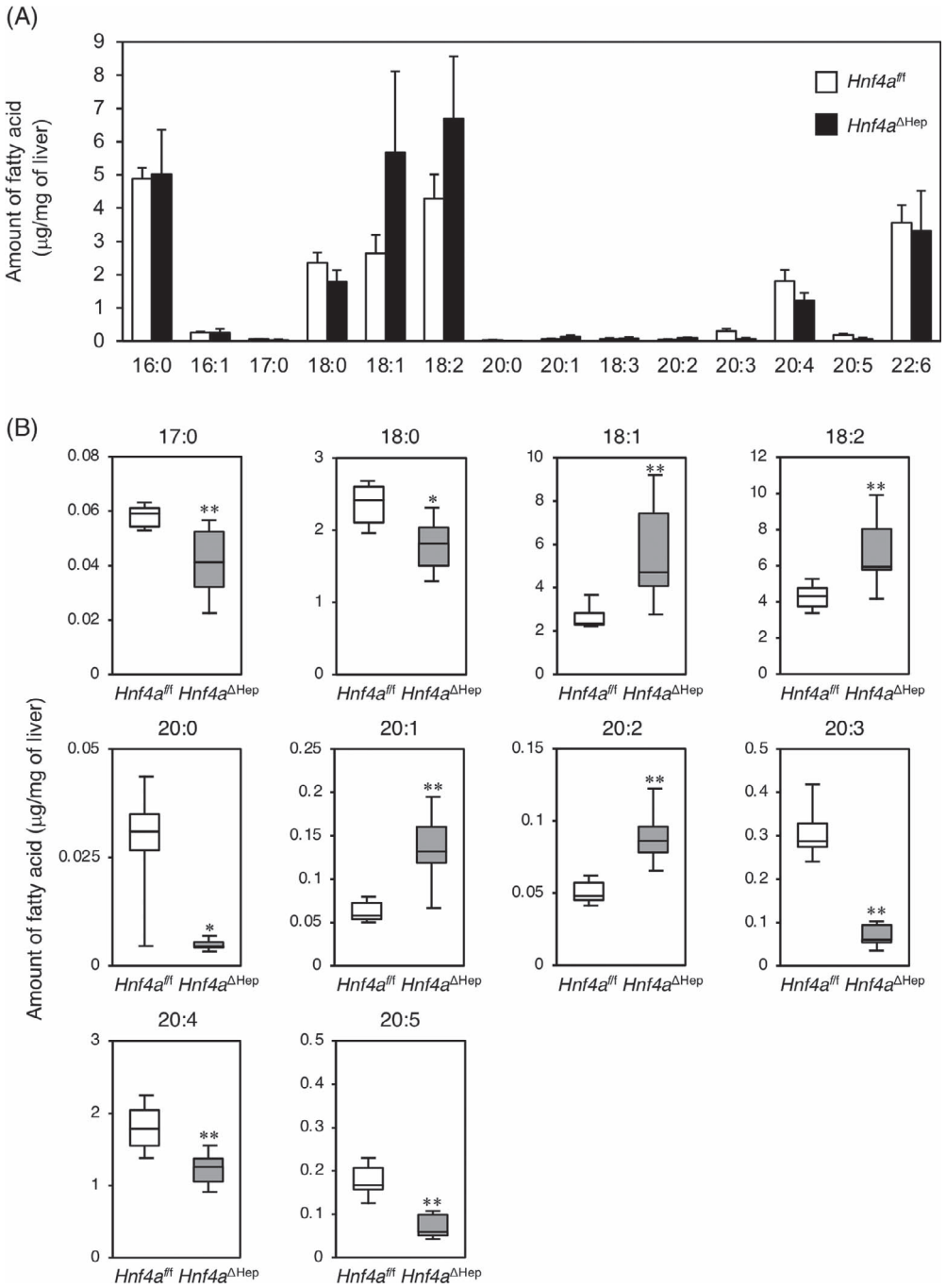

Fig. 6. FA compostion in the livers of *Hnf4a* $^{f/f}$ *and Hnf4a* $^{\Delta Hep}$ mice. (A) FA composition of total lipid extracts from *Hnf4a*$^{f/f}$ and *Hnf4a*$^{\Delta Hep}$ mouse liver ($n = 6$ for *Hnf4a*$^{f/f}$ mice, and 8 for *Hnf4a*$^{\Delta Hep}$ mice). Data are mean ± S.D. (B) Box plot of significantly different FAs between *Hnf4a*$^{f/f}$ and *Hnf4a*$^{\Delta Hep}$ mice. *, $P < 0.05$; **, $P < 0.01$ compared to *Hnf4a*$^{f/f}$ mice.

Hnf4a$^{\Delta Hep}$*/Ppara*$^{-/-}$ mice, regulation of *Elovl7* mRNA expression was further investigated. For regulation by PPARα, expression of *Elovl7* mRNA in wild-type mice (*Ppara*$^{+/+}$ mice) was increased about 30-fold by treatment with the PPARα agonist, Wy-14,643, while no induction was observed in Wy-14,643-treated *Ppara*$^{-/-}$ mice, indicating that *Elovl7* is a novel PPARα target gene (Fig. 7C). However, expression of *Elovl7* mRNA was increased as high in *Hnf4a*$^{\Delta Hep}$*/Ppara*$^{-/-}$ mice as in *Hnf4a*$^{\Delta Hep}$ mice, suggesting that *Elovl7* would be negatively regulated by HNF4α. However, expression of *Elovl7* mRNA was not altered by the overexpression and suppression of HNF4α in Huh7 and HepG2 cells (Fig. 7D). In order to investigate whether trasactivation of *Elovl7* is PPARα-dependent, promoter analysis of the *Elovl7* gene was performed (Fig. 7E). Three PPREs were expected between +1074 and + 2182 from the transcription start site in the mouse *Elovl7* gene. The promoter region including this region (PPRE1–3) with herpes simplex virus-TK mini promoter was transactivated by PPARα in the presence of Wy-14,643. The promoter including PPRE2/PPRE3 and PPRE3 alone was also transactivated by PPARα and

Wy-14,643, but the activity was lower than that with all PPREs. The promoter activity of the mutated PPRE3 was almost completely suppressed, indicating that *Elovl7* is directly transactivated by PPARα via PPRE3 between +2168 and + 2182.

Transactivation of the Fatp1 promoter by stearate and oleate

Assuming that FA variation is also involved in PPARα activation in *Hnf4a*$^{\Delta Hep}$ mice, transactivation capacity of PPARα upon addition of C18:0 and C18:1 using the *Fatp1* promoter was investigated. When PPARα and RXRα were co-expressed compared to the empty vectors, further transactivation was observed when both C18:0 and C18:1 were added (Fig. 8A). In addition, comparing the cases with the addition of C18:0 and C18:1, respectively, the addition of C18:1 showed more pronounced transactivation. This indicates that C18:1 has a greater effect on PPARα activation in *Hnf4a*$^{\Delta Hep}$ mice. Since the ratio of C18:1 to C18:0 was increased in *Hnf4a*$^{\Delta Hep}$ mice (C18:1/C18:0 = 3.2 ± 0.4) compared to that in *Hnf4a*$^{f/f}$ mice (C18:1/C18:0 = 1.1 ± 0.2) (Fig. 6), promoter analysis was further examined to determine whether the differences in transactivation ability could be observed in different ratios of C18:0 and C18:1. Higher C18:1/C18:0 ratio (C18:1:C18:0 = 3:1) exhibited significantly greater transactivation capacity than equal C18:1/C18:0 ratio (C18:1:C18:0 = 1:1) (Fig. 8B). These results suggest that elevated C18:1/C18:0 at least partially contributes to PPARα activation in *Hnf4a*$^{\Delta Hep}$ mice.

Discussion

Liver-specific *Hnf4a*-null mice (*Hnf4a*$^{\Delta Hep}$ mice) in the fed state had lower blood glucose levels of approximately 3/4 compared to the control mice. As described previously, HNF4α was found to directly regulate many genes involved in the glucose metabolism pathways of glycolysis, glycogen synthesis and gluconeogenesis, such as pyruvate kinase1 (*Pklr*), pyruvate carboxylase (*Pc*) and glycogen synthase 2 (*Gys2*) *(31–33)*. In addition to the decreased expression of *Pklr*, *Pc* and *Gys2* in *Hnf4a*$^{\Delta Hep}$ mice, expression of glycogen phosphorylase (*Pygl*) was also decreased, revealing that *Hnf4a*$^{\Delta Hep}$ mice could not produce and degrade glycogen in the liver. However, hepatic glycogen levels in *Hnf4a*$^{\Delta Hep}$ mice were normal in the fed state but were higher than those in control *Hnf4a*$^{f/f}$ mice during fasting. These results indicate that *Hnf4a*$^{\Delta Hep}$ should not produce glucose from glycogen because of decreased expression of *Pygl* and glucose 6-phosphatase catalytic subunit (*G6pc1*), an HNF4α target gene *(40)*. Furthermore, the results of pyruvate tolerance test showed that *Hnf4a*$^{\Delta Hep}$ are less active in gluconeogenesis, probably due to decreased expression of *Pc*, *Pepck*1 and *G6pc1*. Despite *Hnf4a*$^{\Delta Hep}$ mice exhibiting low gluconeogenesis, *Hnf4a*$^{\Delta Hep}$ mice maintain normal glucose levels during 16 h fasting. This does not mean that *Hnf4a*$^{\Delta Hep}$ mice cannot use glycogen, but one possible reason to maintain glucose levels during fasting is that they store about 4-fold more liver glycogen during fasting than the control mice. *Hnf4a*$^{\Delta Hep}$ mice may still continue to use glycogen available when glycogen stores were depleted in control mice. However, blood glucose levels in *Hnf4a*$^{\Delta Hep}$ mice in the fed state are low probably due to severely decreased expression of hepatic glucagon receptor (*Gcgr*). Indeed, *Gcgr*-null mice exhibit low blood glucose, improved glucose tolerance and hyperglucagonemia *(41)*, consistent with the phenotypes of *Hnf4a*$^{\Delta Hep}$ mice. Overexpression of HNF4α induced *GCGR* expression in human HCC cell lines that highly express endogenous HNF4α, but inhibition of HNF4α did not suppress *GCGR* expression in these cells. Whether *GCGR* is a direct target gene of HNF4α is unknown and further analyses are required. These results indicate that *Hnf4a*$^{\Delta Hep}$ mice in the fed state exhibit lower blood glucose levels, likely due to decreased expression of *Gcgr*, decreased glucogenesis and decreased glycogenolysis (Fig. 9A). The results of glucose tolerance test showed that *Hnf4a*$^{\Delta Hep}$ mice are more glucose tolerant compared to the control mice. The efficiency of glucose disposal by insulin-mediated glucose uptake and suppression of hepatic glucose production are primary effectors for glucose tolerance. Thus, hypersensitivity to insulin action could explain at least part of glucose tolerance. However, the results of inulin tolerance test clearly show that *Hnf4a*$^{\Delta Hep}$ mice are less insulin sensitive than the controls. *Hnf4a*$^{\Delta Hep}$ mice had a defect in gluconeogenesis, but this is not likely to have a strong effect to reduce fasting glucose levels in *Hnf4a*$^{\Delta Hep}$ mice because fasting glucose levels in *Hnf4a*$^{\Delta Hep}$ mice are the same as in the control mice. Therefore, further investigation of glucose tolerance in *Hnf4a*$^{\Delta Hep}$ mice is needed.

Hnf4a $^{\Delta Hep}$ mice showed lower blood glucose levels and increased hepatic expression of *Pkd4* and *Hmgcs2* in the fed state, indicating that *Hnf4a*$^{\Delta Hep}$ mice use FAs and ketone bodies as an alternative pathway to produce energy. Increased expression of LPL that metabolizes blood TG into FAs, suggesting that FAs are then taken up into hepatocytes by FATP1 and FAT/CD36 encoded by mRNAs increased in *Hnf4a*$^{\Delta Hep}$ mice where they are subjected to FA oxidation pathways to produce energy (Fig. 9B). On the other hand, it was reported that expression of HNF4α target genes *Apob* and *Mttp* are decreased in *Hnf4a*$^{\Delta Hep}$ mice *(4, 36, 37)*, resulting in reduced ability to pack lipid into VLDL and transport it out of the liver (Fig. 9C). Thus, while lipid transport outside the liver decreases, FAs that are taken up by FATP1 and FAT/CD36 are thought to cause lipid accumulation in the liver. Expression of *Cidea* (cell death inducing DFFA like effector A), a target of PPARα that has a critical role in fusion and growth of lipid droplets, is also significantly increased in *Hnf4a*$^{\Delta Hep}$ mice *(42)*. Thus, increased expression of *Cidea* could be involved in the enlargement of lipid droplets that accumulated in *Hnf4a*$^{\Delta Hep}$ mice (Fig. 9D).

Interestingly, hepatic expression of many PPARs target genes involved in FA oxidation were clearly increased in *Hnf4a*$^{\Delta Hep}$ mice. However, PPARα is known to be regulated by HNF4α *(43)*, and expression of *Ppara* mRNA and PPARα protein was largely decreased in *Hnf4a*$^{\Delta Hep}$ mice. In other words, a discrepancy arose when the expression of PPARα was decreased, while the expression of the target genes was increased in *Hnf4a*$^{\Delta Hep}$ mice. Expression of *Fatp1*, an another PPAR target gene *(27)*, was also increased in *Hnf4a*$^{\Delta Hep}$ mice, and PPARα, but not PPARβ and PPARγ, significantly bound to the PPRE in the *Fatp1* promoter. These results strongly suggest that PPARα can be partially activated in *Hnf4a*$^{\Delta Hep}$ mice and is more active

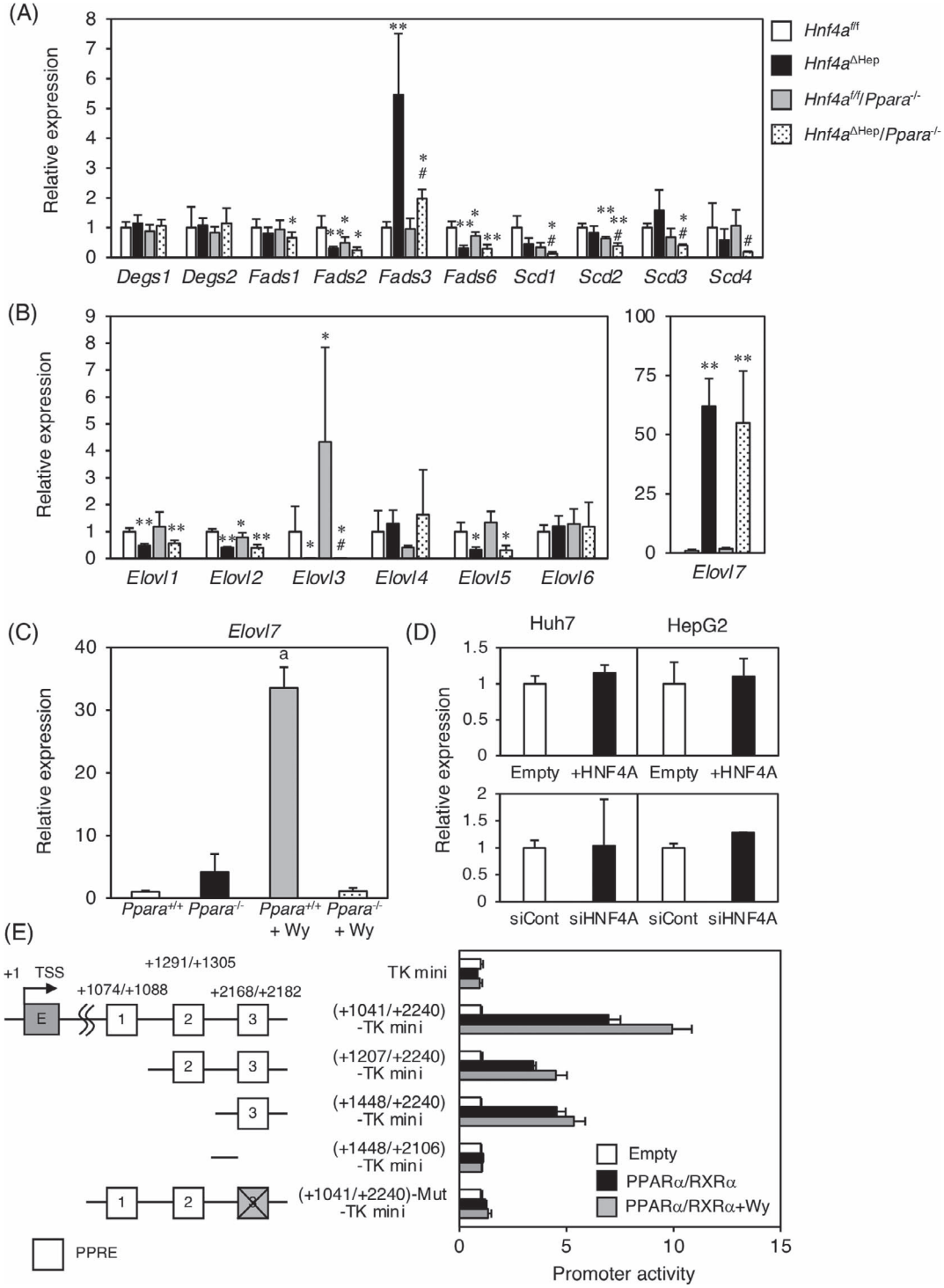

Fig. 7. Expression of FA desaturase and elongases in *Hnf4a*$^{f/f}$ *and Hnf4a*$^{\Delta Hep}$, *Hnf4a*$^{f/f}$*/Ppara*$^{-/-}$, and *Hnf4a*$^{\Delta Hep}$*/Ppara*$^{-/-}$ mice and transactivation of the *Elovl7* promoter. Quantitative RT-PCR of FA desaturases (A) and elongases (B) from total liver RNA of *Hnf4a*$^{f/f}$, *Hnf4a*$^{\Delta Hep}$, *Hnf4a*$^{f/f}$*/Ppara*$^{-/-}$, and *Hnf4a*$^{\Delta Hep}$*/Ppara*$^{-/-}$ mice ($n = 5$ for each genotype). Data are mean ± S.D. *, $P < 0.05$; **, $P < 0.01$ compared to *Hnf4a*$^{f/f}$ mice. #, $P < 0.05$ compared to *Hnf4a*$^{\Delta Hep}$ mice. (C) Quantitative RT-PCR of *Elovl7* in *Ppara*$^{+/+}$ and *Hnf4a*$^{\Delta Hep}$*/Ppara*$^{-/-}$ mice fed 0.1%Wy-14,643 for 3 days. The normalized expression is presented relative to that in *Ppara*$^{+/+}$ mice. Data are mean ± S.D. [a], $P < 0.01$ compared to *Ppara*$^{+/+}$ mice. (D) Quantitative RT-PCR from total RNA of HepG2 and Huh7 cells transfected empty and HNF4α (*upper*), and negative control of siRNA (siCont) and siRNA for HNF4α (siHNF4A) (*lower*). The normalized expression in the cells transfected HNF4α expression vector and siHNF4A is presented relative to that in the cells transfected empty vector and siCont. (E) Promoter activity of the mouse *Elovl7* gene. The *Elovl7* promoters with the HSV-TK-mini promoter were co-transfected with empty vector (Empty) and PPARα and RXRα expression vectors with and without 10 μM Wy-14,643 (PPARα/RXRα and PPARα/RXRα + Wy) into HEK293T cells. Mutations were introduced into PPRE3 in the promoter (gray square with a cross). Data are mean ± S.D. The normalized activity ± S.D. was presented as relative activity based on empty vector-transfected cells.

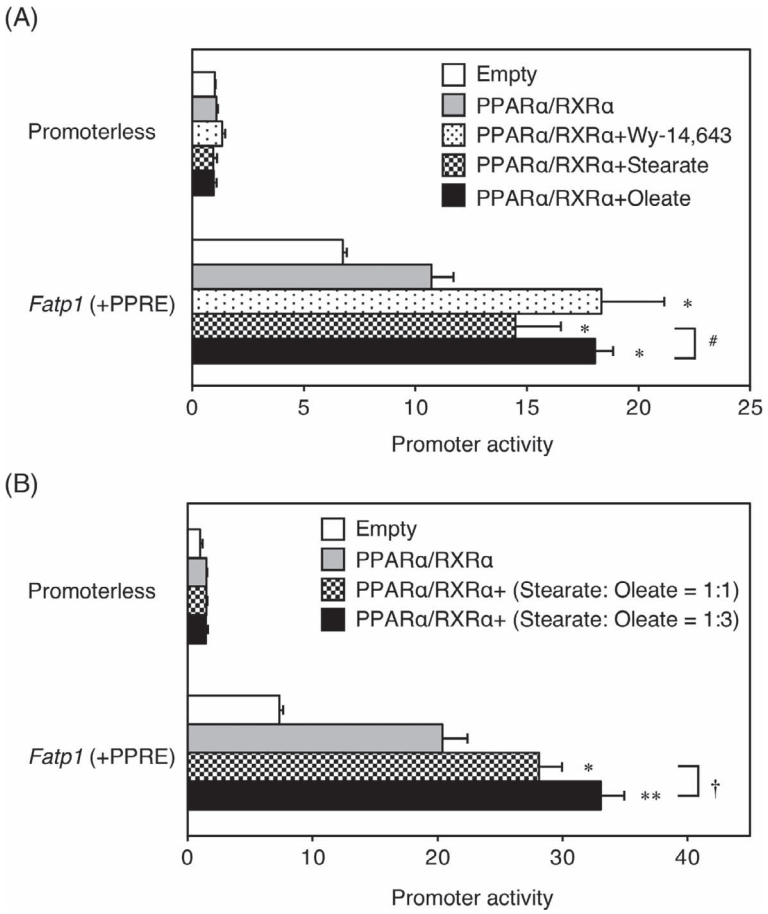

Fig. 8. Promoter analysis of the *Fatp1* gene in the presence of C18:0 and C18:1. (A) Promoter activity of the *Fatp1* gene. The *Fatp1* promoter with PPRE was co-transfected with empty vector (Empty), PPARα and RXRα expression vectors (PPARα/RXRα) with or without 10 μM Wy-14,643 (PPARα/RXRα + Wy-14,643), 50 μM C18:0 (PPARα/RXRα + stearate), and 50 μM C18:1 (PPARα/RXRα + oleate) into HEK293T cells. Data are mean ± S.D. The normalized activity ± S.D. was presented as relative activity based on empty vector-transfected cells. *, $P < 0.05$ compared to PPARα/RXRα expression vectors-transfected cells. #, $P < 0.05$ compared to PPARα/RXRα expression vectors-transfected cells with stearate. (B) The *Fatp1* promoter with PPRE was co-transfected with empty vector (Empty), PPARα and RXRα expression vectors (PPARα/RXRα + BSA) with or without 25 μM stearate and 25 μM oleate (PPARα/RXRα + stearate + oleate = 1:1), or 12.5 μM stearate and 37.5 μM oleate (PPARα/RXRα + stearate + oleate = 1:3) into HEK293T cells. Data are mean ± S.D. The normalized activity ± S.D. was presented as relative activity based on empty vector-transfected cells. *, $P < 0.05$; **, $P < 0.01$ compared to PPARα/RXRα expression vectors-transfected cells with BSA. †, $P < 0.05$ compared to PPARα/RXRα expression vectors-transfected cells with stearate and oleate (1:1).

than the corresponding higher levels of PPARα in wild-type *Hnf4a*$^{f/f}$ mice, and that activated PPARα transactivate the expression of PPAR target genes. To support this view, *Ppara*$^{-/-}$/*Hnf4a*$^{\Delta Hep}$ had improved hepatosteatosis and liver fibrosis, and decreased expression of genes involved in inflammation, oxidative stress and fibrosis.

In addition, increased expression of PGC1α, a coactivator of PPARs *(44–46)*, was observed in *Hnf4a*$^{\Delta Hep}$ mice. PGC1α and PPARα were reported to interact and induce the expression of FA β-oxidation-related genes *(47, 48)*, suggesting that PGC1α strongly affects PPARα function in the liver. Transactivation of *Fatp1* by PPARα was PPRE-dependent and further enhanced by PGC1α and its ligand. Similar trends were observed for PPARβ and PPARγ, but the transactivation capacity was much lower than that of PPARα, indicating that PGC1α and the endogenous ligands may be involved in the activation of PPARα in *Hnf4a*$^{\Delta Hep}$ mice (Fig. 9E).

Changes in the composition of endogenous FAs as PPARα ligands that may account for another factor in activation of PPARα, was also examined. Of the FAs that showed significant variation in *Hnf4a*$^{\Delta Hep}$ mice, C18:1 was reported to activate PPARγ signaling higher than C18:0 *(49)*. Promoter analysis of *Fatp1* having a functional PPRE showed that C18:1 enhanced the transactivation capacity of PPARα compared to C18:0. Since the C18:1/C18:0 ratio was elevated in *Hnf4a*$^{\Delta Hep}$ mice, co-addition of C18:0 and C18:1 resulted in stronger transactivation when the ratio of C18:1 was higher, as observed in *Hnf4a*$^{\Delta Hep}$ mouse liver. These results suggest that the activation of PPARα in *Hnf4a*$^{\Delta Hep}$ mice is partially related to increased expression of *Pgc1a*, a coactivator of all PPARs, as well as increased C18:1 and/or C18:1/C18:0 ratio (Fig. 9F). C18:1 was reported to be also increased, but C18:0 remain unchanged in liver-specific *Hnf4a*-knockdown mice that were generated by injecting AAV8-TGB-Cre into *Hnf4a*$^{f/f}$ mice *(50)*. Since the physiological effects elicited by AAV8 injection on mice was reported to be minimal *(51)*, the difference may be due to the fact that the time HNF4α is being knocked-down using AAV8-TGB-Cre is clearly longer than in the *Hnf4a*$^{\Delta Hep}$ mice used in this study.

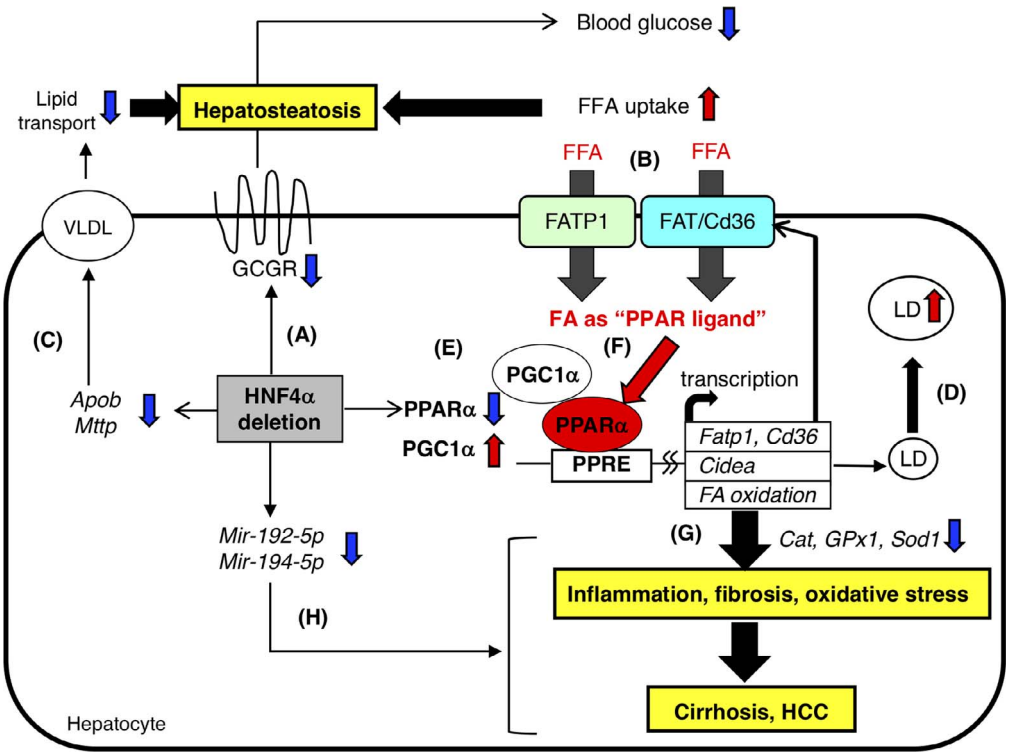

Fig. 9. Schematic diagram of NAFLD development in *Hnf4a* $^{\Delta Hep}$ mice. (A) Decreased expression of *Gcgr* induces lowered glucose levels due to decreased glucogenesis. (B) Increased expression of *Fatp1* and *Fat/Cd36* with *Lpl* promotes uptake of FAs into hepatocyte, which presumably are ligands for PPARα. (C) Decreased expression of *Apob* and *Mttp*, the target genes of HNF4α, suppressed VLDL packing of lipids, resulting in inability to transport lipids out of the liver *(4)*. (D) Increased expression of *Cidea*, the target gene of HNF4α, promotes enlargement of lipid droplets *(42)*. (E) Increased expression of *Pgc1a* promotes PPARα transactivation. (F) Activation of PPARα by increased C18:1 and decreased C18:0 with altered expression of FA desaturases and elongases. (G) Decreased expression of *Mir-194-5p* and *Mir-192-5p*, the target genes of HNF4α, promotes cell malignancy *(29)*. (H) Accumulation of oxidative stress by increased expression of PPARα target genes involved in FA oxidation and decreased expression of genes encoding antioxidant enzymes *(5)*.

Since ELOVL1, ELOVL3 and ELOVL7 are involved in the elongation from C18:0 to C20:0 *(52)*, decreased C18:0 and C20:0 in *Hnf4a*$^{\Delta Hep}$ mice might be due to lower expression of *Elovl1* and *Elovl3*. Hepatic expression of *Elovl7* mRNA was increased more than 50-fold in *Hnf4a*$^{\Delta Hep}$ mice, but the elongation activity using C18:0 as a substrate was reported to be the highest for ELOVL3, and the activity of ELOVL3 is about 6-fold higher than that of ELOVL7 that is not significantly expressed in the liver *(52, 53)*. In addition, since *Elovl3* expression is rarely observed in *Hnf4a*$^{\Delta Hep}$ mice, the reduction of C20:0 is likely to be largely due to reduced expression of *Elovl3* in *Hnf4a*$^{\Delta Hep}$ mice.

Of the monounsaturated FAs, C18:1 and C20:1 were increased in *Hnf4a*$^{\Delta Hep}$ mice. The desaturation reaction from C18:0 to C18:1 is mediated by the Δ9-desaturases SCD1, SCD2 and SCD4 *(54)*. However, since no significant expression change of these mRNAs was observed in *Hnf4a*$^{\Delta Hep}$ mice, the reasons for the elevated C18:1 need further verification including analysis of SCD activity in the liver. The elevated C20:1 in *Hnf4a*$^{\Delta Hep}$ mice might be due to the increased substrate C18:1 and the increased expression of *Elovl7*, but the elongation activity was slightly elevated because ELOVL3, that has reduced expression in *Hnf4a*$^{\Delta Hep}$ mice, is more active than ELOVL7 *(52)*. Four n-6 polyunsaturated FAs were detected. Of these, C18:2 and C20:2 were significantly increased, while C20:3 and C20:4 were decreased. FADS2 is responsible for the desaturation from C20:2 to C20:3 *(55)*, but its expression is decreased in *Hnf4a*$^{\Delta Hep}$ mice. The result would have been a decrease of C20:3 and subsequent C20:4, accompanied by an increase of the substrate, C18:2 and C20:2. Three n-3 polyunsaturated FAs were detected of which C20:5 was significantly decreased in *Hnf4a*$^{\Delta Hep}$ mice. This may be due to the lower expression of *Fads2* and *Elovl5*, that encode enzymes responsible for the elongation and unsaturation leading to C20:5, in *Hnf4a*$^{\Delta Hep}$ mice.

Liver tissue staining showed improved lipid accumulation in *Hnf4a*$^{\Delta Hep}$*/Ppara*$^{-/-}$ mice compared to *Hnf4a*$^{\Delta Hep}$ mice. This may be partly due to the significantly decreased expression of *Scd1* in *Hnf4a*$^{\Delta Hep}$*/Ppara*$^{-/-}$ mice compared to *Hnf4a*$^{\Delta Hep}$ mice. *Scd1*-nulll mice had significantly decreased hepatic cholesterol ester and triglyceride levels *(56)*. It was also reported that the C18:1/C18:0 ratio of total liver lipids and the amount of C18:1 is decreased in *Scd1*-nulll mice and C18:1 may have contributed to hepatosteatosis *(56, 57)*. Thus, decreased expression of *Scd1* in *Hnf4a*$^{\Delta Hep}$*/Ppara*$^{-/-}$ mice may partially lead to the improvement of hepatosteatosis in *Hnf4a*$^{\Delta Hep}$ mice.

Since miR-192-5p and 194-5p are novel HNF4α target miRNA genes and many of the identified target genes are involved in cell malignancy *(29)*, these miRNAs are expected to be involved in the development of NAFLD to NASH and HCC (Fig. 9G).

Various animal models of NAFLD/NASH have been used, and mice and rats fed methionine-choline-deficient (MCD) diet are the dietary models *(58, 59)*. In addition

to steatohepatitis, invasion of inflammatory cells, hepatocyte necrosis and local fibrosis was observed in the MCD diet model. In addition to dietary models, single gene mutated models such as *ob/ob* and *db/db* mice and various gene modified models containing *Apoe2*-KI mice fed high-fat diet (HFD) have been also used *(23, 60, 61)*. These animal models reflect similar pathogenesis of NAFLD/NASH, but they also differ from human NAFLD/NASH with diverse background factors that vary greatly among individuals. NAFLD/NASH is often associated with obesity and insulin resistance, but MCD-fed mice are neither obese nor insulin resistance *(58, 59, 62)*. Although obesity is undoubtedly the major risk factor for NAFLD/NASH, many clinical observations showed the existence of lean NAFLD/NASH patients with normal body mass index *(63, 64)*. Phosphatidylethanolamine *N*-methyltransferase (*Pemt*)-deficient mice fed high fat-high sucrose diet exhibit fatty livers and progress to NASH without obesity and diabetes, and hepatic expression of *Pemt* was lower in lean NASH patient without obesity *(65)*. In addition, hepatic expression of HNF4α protein in *Pemt*-deficient mice was suppressed by hypermethylation of the genomic DNA region. Further analysis is needed to determine whether *Hnf4a*$^{\Delta Hep}$ mice develop NASH, but *Hnf4a*$^{\Delta Hep}$ mice show neither obesity nor diabetes, indicating that *Hnf4a*$^{\Delta Hep}$ mice are at least classified as lean NAFLD without obesity and diabetes.

Studies using various animal models of NAFLD/NASH have reported an association between PPARα and NASH. Treatment of MCD-fed mice with a PPARα agonist was shown to improve lipid and peroxide accumulation in the liver and protect against steatohepatitis *(22)*. Others reported that treatment of *Apoe2*-KI mice fed HFD with fenofibrate protects against hepatosteatosis and hepatic macrophage accumulation via activation of PPARα *(23)*. These studies suggest that PPARα agonists may be useful in the treatment of NAFLD/NASH. In fact, clinical trials in patients with NAFLD/NASH are underway, with positive results, although some are still in the process of being validated *(66–68)*. In addition, a common finding reported in the above mouse models is that NASH-like phenotype is exacerbated when PPARα is deficient. On the other hand, hepatosteatosis and fibrosis in *Hnf4a*$^{\Delta Hep}$ mice in this study were ameliorated by loss of PPARα. In fact, increased expression of oxidative stress markers was observed in *Hnf4a*$^{\Delta Hep}$ mice. Conversely, the expression of catalase (*Cat*), *Sod1* and *Gpx1* mRNAs encoding proteins that function as antioxidants, was decreased in *Hnf4a*$^{\Delta Hep}$ mice *(5)*. These results support the idea that ovidative stress may accumulate in *Hnf4a*$^{\Delta Hep}$ mouse livers. Thus, increased oxidative stress in *Hnf4a*$^{\Delta Hep}$ mice may partially lead to the exacerbation of NAFLD (Fig. 9H).

It is also thought that decreased uptake of lipids into VLDL and secretion out of hepatocytes caused by the lower expression of *Apob* and *Mttp* and the uptake of lipids by increased *Fatp1* and *Fat/Cd36* results in excess lipids in the liver which exceed the processing capacity by β-oxidation, in turn causing lipid accumulation. In addition, the expression of genes encoding antioxidant enzymes, including catalase *(5)*, is decreased in *Hnf4a*$^{\Delta Hep}$ mice, suggesting that oxidative stress is increasing. Thus, *Hnf4a*$^{\Delta Hep}$ mice present a different model from previously utilized NAFLD models and will provide a new perspective for future NAFLD research. However, HNF4α regulates the expression of a vast array of genes involved in liver function. For example, elevated plasma bile acid levels in NASH patients and elevated serum bile acid levels in lean NAFLD patients were reported *(69, 70)*. *Hnf4a*$^{\Delta Hep}$ mice exhibit elevated serum bile acids *(6)*, which may be consistent with these reports. Conversely, elevated serum iron levels in NAFLD patients and an association between iron accumulation in the liver and exacerbation of NAFLD are inconsistent with the fact that *Hnf4a*$^{\Delta Hep}$ mice show hypoferremia and no change in iron levels in the liver *(5, 71, 72)*. These phenotypes in *Hnf4a*$^{\Delta Hep}$ mice are caused by decreased expression of direct target genes of HNF4α. Thus, *Hnf4a*$^{\Delta Hep}$ mice are heavily influenced by HNF4α, which may be difficult to apply to the mechanism of NAFLD development in wild-type mice as well as humans. Further analyses are required to elucidate the detailed mechanism of NAFLD development in *Hnf4a*$^{\Delta Hep}$ mice.

Funding

This work was supported by grants from the Ministry of Education, Culture, Sports, Science, and Technology of Japan (Grant-in-Aid for Scientific Research, No. 16K08728 to Y.I., 19K07474 to Y.I.); Gunma University, Akita University, Nagoya University, Collaborative Investigation Project, the joint research program of the Institute for Molecular and Cellular Regulation, Gunma University (No. 20009 to Y.I.); Bristol-Meyers Squibb to Y.I.; and Takeda Science Foundation to Y.I.

Data availability

All the data presented in the manuscript is provided in the main text and the supplementary file.

Author contributions

CI.K.-C: Conceptualization, Data Curation, Formal Analysis, Methodology, Validation, Writing—Original Draft, Visualization. M.T.: Investigation, Visualization. C.S.: Investigation. N.O.: Methodology, Software, Resources. T.I.: Resources. W.I.: Investigation. Y.S.: Investigation. S.I.T.: Investigation. Y.N.: Methodology, Investigation. Y.F.: Resources. R.Y.: Investigation. M.S.: Resources. F.J.G.: Resources, Writing—Review and Editing. Y.I.: Project Administration, Writing—Review and editing, Supervision, Project Administration, Funding acquisition.

Conflicts of interest

None declared.

Acknowledgements

We acknowledge Dr. Oksana Gavrilova (Mouse Metabolism Core Laboratory, National Institute of Diabetes and Digestive and Kidney Diseases, National Institutes of Health, Bethesda, MD) and members of the Inoue Laboratory for serum analysis, and discussions and comments on the manuscript.

Supplementary material

Supplementary Data are available at *JB Online*.

REFERENCES

1. Lau, H.H., Ng, N.H.J., Loo, L.S.W., Jasmen, J.B., and Teo, A.K.K. (2018) The molecular functions of hepatocyte nuclear factors - in and beyond the liver. *J. Hepatol.* **68**, 1033–1048
2. Watt, A.J., Garrison, W.D., and Duncan, S.A. (2003) HNF4: a central regulator of hepatocyte differentiation and function. *Hepatology* **37**, 1249–1253
3. Odom, D.T., Zizlsperger, N., Gordon, D.B., Bell, G.W., Rinaldi, N.J., Murray, H.L., Volkert, T.L., Schreiber, J., Rolfe, P.A., Gifford, D.K., Fraenkel, E., Bell, G.I., and Young, R.A. (2004) Control of pancreas and liver gene expression by HNF transcription factors. *Science* **303**, 1378–1381
4. Hayhurst, G.P., Lee, Y.H., Lambert, G., Ward, J.M., and Gonzalez, F.J. (2001) Hepatocyte nuclear factor 4α (nuclear receptor 2A1) is essential for maintenance of hepatic gene expression and lipid homeostasis. *Mol. Cell. Biol.* **21**, 1393–1403
5. Matsuo, S., Ogawa, M., Muckenthaler, M.U., Mizui, Y., Sasaki, S., Fujimura, T., Takizawa, M., Ariga, N., Ozaki, H., Sakaguchi, M., Gonzalez, F.J., and Inoue, Y. (2015) Hepatocyte nuclear factor 4α controls iron metabolism and regulates transferrin receptor 2 in mouse liver. *J. Biol. Chem.* **290**, 30855–30865
6. Inoue, Y., Yu, A.M., Yim, S.H., Ma, X., Krausz, K.W., Inoue, J., Xiang, C.C., Brownstein, M.J., Eggertsen, G., Bjorkhem, I., and Gonzalez, F.J. (2006) Regulation of bile acid biosynthesis by hepatocyte nuclear factor 4α. *J. Lipid Res.* **47**, 215–227
7. Inoue, Y., Hayhurst, G.P., Inoue, J., Mori, M., and Gonzalez, F.J. (2002) Defective ureagenesis in mice carrying a liver-specific disruption of hepatocyte nuclear factor 4α (HNF4α). HNF4α regulates ornithine transcarbamylase in vivo. *J. Biol. Chem.* **277**, 25257–25265
8. Huang, K.W., Reebye, V., Czysz, K., Ciriello, S., Dorman, S., Reccia, I., Lai, H.S., Peng, L., Kostomitsopoulos, N., Nicholls, J., Habib, R.S., Tomalia, D.A., Saetrom, P., Wilkes, E., Cutillas, P., Rossi, J.J., and Habib, N.A. (2020) Liver activation of hepatocellular nuclear factor-4α by small activating RNA rescues dyslipidemia and improves metabolic profile. *Mol Ther Nucleic Acids* **19**, 361–370
9. Chalasani, N., Younossi, Z., Lavine, J.E., Charlton, M., Cusi, K., Rinella, M., Harrison, S.A., Brunt, E.M., and Sanyal, A.J. (2018) The diagnosis and management of nonalcoholic fatty liver disease: Practice guidance from the American Association for the Study of Liver Diseases. *Hepatology* **67**, 328–357
10. Chalasani, N., Younossi, Z., Lavine, J. E., Diehl, A. M., Brunt, E. M., Cusi, K., Charlton, M., Sanyal, A. J., American Association for the Study of Liver, D., American College of, G., and American Gastroenterological, A (2012) The diagnosis and management of non-alcoholic fatty liver disease: Practice guideline by the American Association for the Study of Liver Diseases, American College of Gastroenterology, and the American Gastroenterological Association. *Am. J. Gastroenterol.* **107**, 811–826
11. Younossi, Z.M., Koenig, A.B., Abdelatif, D., Fazel, Y., Henry, L., and Wymer, M. (2016) Global epidemiology of nonalcoholic fatty liver disease-Meta-analytic assessment of prevalence, incidence, and outcomes. *Hepatology* **64**, 73–84
12. Day, C.P., and James, O.F. (1998) Steatohepatitis: a tale of two "hits"? *Gastroenterology* **114**, 842–845
13. Tilg, H., and Moschen, A.R. (2010) Evolution of inflammation in nonalcoholic fatty liver disease: the multiple parallel hits hypothesis. *Hepatology* **52**, 1836–1846
14. Puri, P., Baillie, R.A., Wiest, M.M., Mirshahi, F., Choudhury, J., Cheung, O., Sargeant, C., Contos, M.J., and Sanyal, A.J. (2007) A lipidomic analysis of nonalcoholic fatty liver disease. *Hepatology* **46**, 1081–1090
15. Matsuzaka, T., Atsumi, A., Matsumori, R., Nie, T., Shinozaki, H., Suzuki-Kemuriyama, N., Kuba, M., Nakagawa, Y., Ishii, K., Shimada, M., Kobayashi, K., Yatoh, S., Takahashi, A., Takekoshi, K., Sone, H., Yahagi, N., Suzuki, H., Murata, S., Nakamuta, M., Yamada, N., and Shimano, H. (2012) Elovl6 promotes nonalcoholic steatohepatitis. *Hepatology* **56**, 2199–2208
16. Baciu, C., Pasini, E., Angeli, M., Schwenger, K., Afrin, J., Humar, A., Fischer, S., Patel, K., Allard, J., and Bhat, M. (2017) Systematic integrative analysis of gene expression identifies HNF4A as the central gene in pathogenesis of non-alcoholic steatohepatitis. *PLoS One* **12**, e0189223
17. Xu, Y., Zalzala, M., Xu, J., Li, Y., Yin, L., and Zhang, Y. (2015) A metabolic stress-inducible miR-34a-HNF4alpha pathway regulates lipid and lipoprotein metabolism. *Nat. Commun.* **6**, 7466
18. Kliewer, S.A., Forman, B.M., Blumberg, B., Ong, E.S., Borgmeyer, U., Mangelsdorf, D.J., Umesono, K., and Evans, R.M. (1994) Differential expression and activation of a family of murine peroxisome proliferator-activated receptors. *Proc. Natl. Acad. Sci. U. S. A.* **91**, 7355–7359
19. Krey, G., Braissant, O., L'Horset, F., Kalkhoven, E., Perroud, M., Parker, M.G., and Wahli, W. (1997) Fatty acids, eicosanoids, and hypolipidemic agents identified as ligands of peroxisome proliferator-activated receptors by coactivator-dependent receptor ligand assay. *Mol. Endocrinol.* **11**, 779–791
20. Grygiel-Gorniak, B. (2014) Peroxisome proliferator-activated receptors and their ligands: nutritional and clinical implications–a review. *Nutr. J.* **13**, 17, Peroxisome proliferator-activated receptors and their ligands: nutritional and clinical implications - a review
21. Ip, E., Farrell, G.C., Robertson, G., Hall, P., Kirsch, R., and Leclercq, I. (2003) Central role of PPARα-dependent hepatic lipid turnover in dietary steatohepatitis in mice. *Hepatology* **38**, 123–132
22. Ip, E., Farrell, G., Hall, P., Robertson, G., and Leclercq, I. (2004) Administration of the potent PPARα agonist, Wy-14,643, reverses nutritional fibrosis and steatohepatitis in mice. *Hepatology* **39**, 1286–1296
23. Shiri-Sverdlov, R., Wouters, K., van Gorp, P.J., Gijbels, M.J., Noel, B., Buffat, L., Staels, B., Maeda, N., van Bilsen, M., and Hofker, M.H. (2006) Early diet-induced non-alcoholic steatohepatitis in APOE2 knock-in mice and its prevention by fibrates. *J. Hepatol.* **44**, 732–741
24. Lalloyer, F., Wouters, K., Baron, M., Caron, S., Vallez, E., Vanhoutte, J., Bauge, E., Shiri-Sverdlov, R., Hofker, M., Staels, B., and Tailleux, A. (2011) Peroxisome proliferator-activated receptor-α gene level differently affects lipid metabolism and inflammation in apolipoprotein E2 knock-in mice. *Arterioscler. Thromb. Vasc. Biol.* **31**, 1573–1579
25. Toyama, T., Nakamura, H., Harano, Y., Yamauchi, N., Morita, A., Kirishima, T., Minami, M., Itoh, Y., and Okanoue, T. (2004) PPARα ligands activate antioxidant enzymes and suppress hepatic fibrosis in rats. *Biochem. Biophys. Res. Commun.* **324**, 697–704
26. Lee, S.S., Pineau, T., Drago, J., Lee, E.J., Owens, J.W., Kroetz, D.L., Fernandez-Salguero, P.M., Westphal, H., and Gonzalez, F.J. (1995) Targeted disruption of the α isoform of the peroxisome proliferator-activated receptor gene in mice results in abolishment of the pleiotropic effects of peroxisome proliferators. *Mol. Cell. Biol.* **15**, 3012–3022

27. Frohnert, B.I., Hui, T.Y., and Bernlohr, D.A. (1999) Identification of a functional peroxisome proliferator-responsive element in the murine fatty acid transport protein gene. *J. Biol. Chem.* **274**, 3970–3977
28. Inoue, Y., Inoue, J., Lambert, G., Yim, S.H., and Gonzalez, F.J. (2004) Disruption of hepatic C/EBPα results in impaired glucose tolerance and age-dependent hepatosteatosis. *J. Biol. Chem.* **279**, 44740–44748
29. Morimoto, A., Kannari, M., Tsuchida, Y., Sasaki, S., Saito, C., Matsuta, T., Maeda, T., Akiyama, M., Nakamura, T., Sakaguchi, M., Nameki, N., Gonzalez, F.J., and Inoue, Y. (2017) An HNF4α-microRNA-194/192 signaling axis maintains hepatic cell function. *J. Biol. Chem.* **292**, 10574–10585
30. Bligh, E.G., and Dyer, W.J. (1959) A rapid method of total lipid extraction and purification. *Can. J. Biochem. Physiol.* **37**, 911–917
31. Yamada, K., Tanaka, T., and Noguchi, T. (1997) Members of the nuclear factor 1 family and hepatocyte nuclear factor 4 bind to overlapping sequences of the L-II element on the rat pyruvate kinase L gene promoter and regulate its expression. *Biochem. J.* **324** (Pt 3), 917–925
32. Chavalit, T., Rojvirat, P., Muangsawat, S., and Jitrapakdee, S. (2013) Hepatocyte nuclear factor 4α regulates the expression of the murine pyruvate carboxylase gene through the HNF4-specific binding motif in its proximal promoter. *Biochim. Biophys. Acta* **1829**, 987–999
33. Mandard, S., Stienstra, R., Escher, P., Tan, N.S., Kim, I., Gonzalez, F.J., Wahli, W., Desvergne, B., Muller, M., and Kersten, S. (2007) Glycogen synthase 2 is a novel target gene of peroxisome proliferator-activated receptors. *Cell. Mol. Life Sci.* **64**, 1145–1157
34. Marra, F., and Tacke, F. (2014) Roles for chemokines in liver disease. *Gastroenterology* **147**, 577–594 e571, 577, 594.e1
35. Masarone, M., Rosato, V., Dallio, M., Gravina, A.G., Aglitti, A., Loguercio, C., Federico, A., and Persico, M. (2018) Role of oxidative stress in pathophysiology of nonalcoholic fatty liver disease. *Oxidative Med. Cell. Longev.* **2018**, 9547613
36. Ladias, J.A., Hadzopoulou-Cladaras, M., Kardassis, D., Cardot, P., Cheng, J., Zannis, V., and Cladaras, C. (1992) Transcriptional regulation of human apolipoprotein genes ApoB, ApoCIII, and ApoAII by members of the steroid hormone receptor superfamily HNF-4, ARP-1, EAR-2, and EAR-3. *J. Biol. Chem.* **267**, 15849–15860
37. Sheena, V., Hertz, R., Nousbeck, J., Berman, I., Magenheim, J., and Bar-Tana, J. (2005) Transcriptional regulation of human microsomal triglyceride transfer protein by hepatocyte nuclear factor-4α. *J. Lipid Res.* **46**, 328–341
38. Schoonjans, K., Peinado-Onsurbe, J., Lefebvre, A.M., Heyman, R.A., Briggs, M., Deeb, S., Staels, B., and Auwerx, J. (1996) PPARα and PPARgamma activators direct a distinct tissue-specific transcriptional response via a PPRE in the lipoprotein lipase gene. *EMBO J.* **15**, 5336–5348
39. Sato, O., Kuriki, C., Fukui, Y., and Motojima, K. (2002) Dual promoter structure of mouse and human fatty acid translocase/CD36 genes and unique transcriptional activation by peroxisome proliferator-activated receptor α and gamma ligands. *J. Biol. Chem.* **277**, 15703–15711
40. Boustead, J.N., Stadelmaier, B.T., Eeds, A.M., Wiebe, P.O., Svitek, C.A., Oeser, J.K., and O'Brien, R.M. (2003) Hepatocyte nuclear factor-4 alpha mediates the stimulatory effect of peroxisome proliferator-activated receptor gamma coactivator-1 alpha (PGC-1 alpha) on glucose-6-phosphatase catalytic subunit gene transcription in H4IIE cells. *Biochem. J.* **369**, 17–22
41. Gelling, R.W., Du, X.Q., Dichmann, D.S., Romer, J., Huang, H., Cui, L., Obici, S., Tang, B., Holst, J.J., Fledelius, C., Johansen, P.B., Rossetti, L., Jelicks, L.A., Serup, P., Nishimura, E., and Charron, M.J. (2003) Lower blood glucose, hyperglucagonemia, and pancreatic α cell hyperplasia in glucagon receptor knockout mice. *Proc. Natl. Acad. Sci. U. S. A.* **100**, 1438–1443
42. Kasano-Camones, C.I., Takizawa, M., Iwasaki, W., Sasaki, S., Hamada, M., Morimoto, A., Sakaguchi, M., Gonzalez, F.J., and Inoue, Y. (2020) Synergistic regulation of hepatic Fsp27b expression by HNF4α and CREBH. *Biochem. Biophys. Res. Commun.* **530**, 432–439
43. Pineda Torra, I., Jamshidi, Y., Flavell, D.M., Fruchart, J.C., and Staels, B. (2002) Characterization of the human PPARalpha promoter: identification of a functional nuclear receptor response element. *Mol. Endocrinol.* **16**, 1013–1028
44. Vega, R.B., Huss, J.M., and Kelly, D.P. (2000) The coactivator PGC-1 cooperates with peroxisome proliferator-activated receptor α in transcriptional control of nuclear genes encoding mitochondrial fatty acid oxidation enzymes. *Mol. Cell. Biol.* **20**, 1868–1876
45. Wang, Y.X., Lee, C.H., Tiep, S., Yu, R.T., Ham, J., Kang, H., and Evans, R.M. (2003) Peroxisome-proliferator-activated receptor delta activates fat metabolism to prevent obesity. *Cell* **113**, 159–170
46. Puigserver, P., Wu, Z., Park, C.W., Graves, R., Wright, M., and Spiegelman, B.M. (1998) A cold-inducible coactivator of nuclear receptors linked to adaptive thermogenesis. *Cell* **92**, 829–839
47. Finck, B.N., Gropler, M.C., Chen, Z., Leone, T.C., Croce, M.A., Harris, T.E., Lawrence, J.C., Jr., and Kelly, D.P. (2006) Lipin 1 is an inducible amplifier of the hepatic PGC-1α/PPARα regulatory pathway. *Cell Metab.* **4**, 199–210
48. Li, S., Liu, C., Li, N., Hao, T., Han, T., Hill, D.E., Vidal, M., and Lin, J.D. (2008) Genome-wide coactivation analysis of PGC-1α identifies BAF60a as a regulator of hepatic lipid metabolism. *Cell Metab.* **8**, 105–117
49. Kobayashi, T., and Fujimori, K. (2012) Very long-chain-fatty acids enhance adipogenesis through coregulation of Elovl3 and PPARgamma in 3T3-L1 cells. *Am. J. Physiol. Endocrinol. Metab.* **302**, E1461–E1471
50. Xu, Y., Zhu, Y., Hu, S., Xu, Y., Stroup, D., Pan, X., Bawa, F.C., Chen, S., Gopoju, R., Yin, L., and Zhang, Y. (2021) Hepatocyte nuclear factor 4α prevents the steatosis-to-NASH progression by regulating p53 and bile acid signaling (in mice). *Hepatology* **73**, 2251–2265
51. Kiourtis, C., Wilczynska, A., Nixon, C., Clark, W., May, S., and Bird, T.G. (2021) Specificity and off-target effects of AAV8-TBG viral vectors for the manipulation of hepatocellular gene expression in mice. *Biol Open* **10**, bio058678
52. Ohno, Y., Suto, S., Yamanaka, M., Mizutani, Y., Mitsutake, S., Igarashi, Y., Sassa, T., and Kihara, A. (2010) ELOVL1 production of C24 acyl-CoAs is linked to C24 sphingolipid synthesis. *Proc. Natl. Acad. Sci. U. S. A.* **107**, 18439–18444
53. Tamura, K., Makino, A., Hullin-Matsuda, F., Kobayashi, T., Furihata, M., Chung, S., Ashida, S., Miki, T., Fujioka, T., Shuin, T., Nakamura, Y., and Nakagawa, H. (2009) Novel lipogenic enzyme ELOVL7 is involved in prostate cancer growth through saturated long-chain fatty acid metabolism. *Cancer Res.* **69**, 8133–8140
54. Miyazaki, M., Bruggink, S.M., and Ntambi, J.M. (2006) Identification of mouse palmitoyl-coenzyme A Delta9-desaturase. *J. Lipid Res.* **47**, 700–704
55. Guillou, H., Zadravec, D., Martin, P.G., and Jacobsson, A. (2010) The key roles of elongases and desaturases in mammalian fatty acid metabolism: Insights from transgenic mice. *Prog. Lipid Res.* **49**, 186–199
56. Miyazaki, M., Kim, Y.C., Gray-Keller, M.P., Attie, A.D., and Ntambi, J.M. (2000) The biosynthesis of hepatic cholesterol esters and triglycerides is impaired in mice with a disruption of the gene for stearoyl-CoA desaturase 1. *J. Biol. Chem.* **275**, 30132–30138
57. Listenberger, L.L., Han, X., Lewis, S.E., Cases, S., Farese, R.V., Jr., Ory, D.S., and Schaffer, J.E. (2003) Triglyceride

accumulation protects against fatty acid-induced lipotoxicity. *Proc. Natl. Acad. Sci. U. S. A.* **100**, 3077–3082
58. Weltman, M.D., Farrell, G.C., and Liddle, C. (1996) Increased hepatocyte CYP2E1 expression in a rat nutritional model of hepatic steatosis with inflammation. *Gastroenterology* **111**, 1645–1653
59. Leclercq, I.A., Farrell, G.C., Field, J., Bell, D.R., Gonzalez, F.J., and Robertson, G.R. (2000) CYP2E1 and CYP4A as microsomal catalysts of lipid peroxides in murine nonalcoholic steatohepatitis. *J. Clin. Invest.* **105**, 1067–1075
60. Kishina, M., Koda, M., Kato, J., Tokunaga, S., Matono, T., Sugihara, T., Ueki, M., and Murawaki, Y. (2014) Therapeutic effects of the direct renin inhibitor, aliskiren, on nonalcoholic steatohepatitis in fatty liver Shionogi ob/ob male mice. *Hepatol. Res.* **44**, 888–896
61. Sahai, A., Malladi, P., Pan, X., Paul, R., Melin-Aldana, H., Green, R.M., and Whitington, P.F. (2004) Obese and diabetic db/db mice develop marked liver fibrosis in a model of nonalcoholic steatohepatitis: role of short-form leptin receptors and osteopontin. *Am. J. Physiol. Gastrointest. Liver Physiol.* **287**, G1035–G1043
62. Rinella, M.E., and Green, R.M. (2004) The methionine-choline deficient dietary model of steatohepatitis does not exhibit insulin resistance. *J. Hepatol.* **40**, 47–51
63. Albhaisi, S., Chowdhury, A., and Sanyal, A.J. (2019) Nonalcoholic fatty liver disease in lean individuals. *JHEP Rep* **1**, 329–341
64. Younes, R., and Bugianesi, E. (2019) NASH in Lean Individuals. *Semin. Liver Dis.* **39**, 086–095
65. Nakatsuka, A., Matsuyama, M., Yamaguchi, S., Katayama, A., Eguchi, J., Murakami, K., Teshigawara, S., Ogawa, D., Wada, N., Yasunaka, T., Ikeda, F., Takaki, A., Watanabe, E., and Wada, J. (2016) Insufficiency of phosphatidylethanolamine N-methyltransferase is risk for lean non-alcoholic steatohepatitis. *Sci. Rep.* **6**, 21721
66. Gawrieh, S., Noureddin, M., Loo, N., Mohseni, R., Awasty, V., Cusi, K., Kowdley, K.V., Lai, M., Schiff, E., Parmar, D., Patel, P., and Chalasani, N. (2021) Saroglitazar, a PPAR-α/gamma agonist, for treatment of NAFLD: A randomized controlled double-blind phase 2 trial. *Hepatology* **74**, 1809–1824
67. Nakajima, A., Eguchi, Y., Yoneda, M., Imajo, K., Tamaki, N., Suganami, H., Nojima, T., Tanigawa, R., Iizuka, M., Iida, Y., and Loomba, R. (2021) Randomised clinical trial: Pemafibrate, a novel selective peroxisome proliferator-activated receptor α modulator (SPPARMα), versus placebo in patients with non-alcoholic fatty liver disease. *Aliment. Pharmacol. Ther.* **54**, 1263–1277
68. Prikhodko, V.A., Bezborodkina, N.N., and Okovityi, S.V. (2022) Pharmacotherapy for non-alcoholic fatty liver disease: emerging targets and drug candidates. *Biomedicine* **10**, 274
69. Grzych, G., Chavez-Talavera, O., Descat, A., Thuillier, D., Verrijken, A., Kouach, M., Legry, V., Verkindt, H., Raverdy, V., Legendre, B., Caiazzo, R., Van Gaal, L., Goossens, J.F., Paumelle, R., Francque, S., Pattou, F., Haas, J.T., Tailleux, A., and Staels, B. (2021) NASH-related increases in plasma bile acid levels depend on insulin resistance. *JHEP Rep* **3**, 100222
70. Chen, F., Esmaili, S., Rogers, G.B., Bugianesi, E., Petta, S., Marchesini, G., Bayoumi, A., Metwally, M., Azardaryany, M.K., Coulter, S., Choo, J.M., Younes, R., Rosso, C., Liddle, C., Adams, L.A., Craxi, A., George, J., and Eslam, M. (2020) Lean NAFLD: A Distinct Entity Shaped by Differential Metabolic Adaptation. *Hepatology* **71**, 1213–1227
71. Hoki, T., Miyanishi, K., Tanaka, S., Takada, K., Kawano, Y., Sakurada, A., Sato, M., Kubo, T., Sato, T., Sato, Y., Takimoto, R., Kobune, M., and Kato, J. (2015) Increased duodenal iron absorption through up-regulation of divalent metal transporter 1 from enhancement of iron regulatory protein 1 activity in patients with nonalcoholic steatohepatitis. *Hepatology* **62**, 751–761
72. George, D.K., Goldwurm, S., MacDonald, G.A., Cowley, L.L., Walker, N.I., Ward, P.J., Jazwinska, E.C., and Powell, L.W. (1998) Increased hepatic iron concentration in nonalcoholic steatohepatitis is associated with increased fibrosis. *Gastroenterology* **114**, 311–318